Transforming Growth Factor Induced Protein Promotes NF-Kappa-B Mediated Angiogenesis During Postnatal Lung Development

Min Liu PhD[1], Cristiana Iosef PhD[1], Shailaja Rao PhD[1], Racquel Domingo-Gonzalez[1], Sha Fu MD[1, 2], Paige Snider PhD[3], Simon J. Conway PhD[3], Gray S. Umbach MD[1,4], Sarah C. Heilshorn[5], Ruby E. Dewi[5], Mar J. Dahl[6], Donald M. Null MD[6], Kurt H. Albertine PhD[6], and Cristina M. Alvira MD[1].

[1]Stanford University, Department of Pediatrics, Center for Excellence in Pulmonary Biology, [2] Liuyang People's Hospital, Hunan, China, [3]HB Wells Center for Pediatric Research, Indiana University School of Medicine, Indianapolis, IN 46202, USA, [4]University of Texas Southwestern Medical School, [5]Stanford University, Department of Materials Science & Engineering, [6] Department of Pediatrics, University of Utah School of Medicine.

Address for Correspondence: Cristina M. Alvira, M.D.
Stanford University School of Medicine
Center for Excellence in Pulmonary Biology
770 Welch Road, Suite 435
Palo Alto, CA 94304
Tel: 650-723-7297, FAX: 650-725-0171
Email: calvira@stanford.edu

Running Title: TGFBI Promotes Pulmonary Angiogenesis

Descriptor number: 3.3 Developmental Lung Biology or 14.3 Neonatal Lung Disease & BPD

Word Count: 4288

AJRCMB Articles in Press. Published December 02, 2020 as 10.1165/rcmb.2020-0153OC
Copyright © 2020 by the American Thoracic Society

Subject Codes: Angiogenesis, Developmental Biology. Pulmonary Biology

Contributions: ML, CI, SR, SF, GSU, RD, SCH, and CMA designed and executed studies, analyzed and interpreted results. PS and SJC created the *Tgfbi* null mice. MJD, DMN, and KHA designed and executed the studies on preterm lambs. ML and CMA drafted the manuscript. All authors contributed edits and significant have given final approval for publication and agree to be accountable for the integrity of the information contained in this manuscript.

Support: This work was supported by National Institutes of Health grants HL122918 (CMA) HL148165 (SJC) HL 110002 (KHA), the Stanford Maternal Child Health Institute, Tashia and John Morgridge Faculty Scholar Award (CMA), The Stanford Chemical Engineering Undergraduate Summer Research Program (GSU), The Stanford CJ Huang SAMSUNG Fellowship (SF), and The University of Utah School of Medicine Division of Neonatology (KHA).

This article has an online data supplement, which is accessible from this issue's table of content

online at www.atsjournals.org.

Some of the results of these studies have been previously reported in the form of a preprint (bioRxiv, [29 May 2020] https://doi.org/10.1101/2020.05.28.121871.

AJRCMB Articles in Press. Published December 02, 2020 as 10.1165/rcmb.2020-0153OC
Copyright © 2020 by the American Thoracic Society

Abstract:

Pulmonary angiogenesis is a key driver of alveolarization. Our prior studies showed that nuclear factor kappa-B (NFκB) promotes pulmonary angiogenesis during early alveolarization. However, the mechanisms regulating temporal-specific NFκB activation in the pulmonary vasculature are unknown. To identify mechanisms that activate pro-angiogenic NFκB signaling in the developing pulmonary vasculature. Proteomic analysis of the lung secretome was performed using two-dimensional difference gel electrophoresis (2D-DIGE). NFκB activation and angiogenic function was assessed in primary pulmonary endothelial cells (PEC) and TGFBI-regulated genes identified using RNA-sequencing. Alveolarization and pulmonary angiogenesis was assessed in WT and *Tgfbi* null mice exposed to normoxia or hyperoxia. Lung TGFBI expression was determined in premature lambs supported by invasive and noninvasive respiratory support. Secreted factors from the early alveolar, but not the late alveolar or adult lung, promoted proliferation and migration in quiescent, adult PEC. Proteomic analysis identified transforming growth factor beta-induced protein (TGFBI) as one protein highly expressed by the early alveolar lung that promoted PEC migration by activating NFκB via αvβ3 integrins. RNA-sequencing identified *Csf3* as a TGFBI-regulated gene that enhances nitric oxide production in PEC. Loss of TGFBI in mice exaggerated the impaired pulmonary angiogenesis induced by chronic hyperoxia, and TGFBI expression was disrupted in premature lambs with impaired alveolarization. Our studies identify TGFBI as a developmentally-regulated protein that promotes NFκB-mediated angiogenesis during early alveolarization by enhancing nitric oxide production. We speculate that dysregulation of TGFBI expression may contribute to diseases marked by impaired alveolar and vascular growth.

Abstract Word Count: 242

AJRCMB Articles in Press. Published December 02, 2020 as 10.1165/rcmb.2020-0153OC
Copyright © 2020 by the American Thoracic Society

Key Words: Alveolarization, endothelial migration, colony stimulating factor-3, nitric oxide production, bronchopulmonary dysplasia.

AJRCMB Articles in Press. Published December 02, 2020 as 10.1165/rcmb.2020-0153OC
Copyright © 2020 by the American Thoracic Society

Introduction

In contrast to many organs, significant lung development occurs postnatally. During alveolarization, the final stage of lung development, division of primitive airspaces by secondary septation, and exponential growth of the pulmonary microvasculature by angiogenesis markedly increases gas exchange surface area (1). Angiogenesis is a key driver of alveolarization. Inhibiting angiogenesis impairs alveolarization, while enhancing angiogenesis preserves alveolarization during injury (2, 3). Dysregulated angiogenesis is observed in premature infants with bronchopulmonary dysplasia (BPD), a chronic lung disease characterized by impaired alveolarization that represents the most common complication of extreme prematurity (4). The extension of alveolarization into postnatal life provides an important window of opportunity for lung repair and regeneration (5). Thus, elucidating pathways that promote pulmonary angiogenesis and alveolarization have important clinical implications.

We previously showed that endogenous NFκB activation promotes pulmonary angiogenesis in the early alveolar lung (6). Blocking NFκB in early alveolar pulmonary endothelial cells (PEC) impairs angiogenic function, and pharmacologic inhibition of NFκB in young mice impairs alveolar and vascular growth yet has no effect on adult mice. However, the mechanisms that induce temporal-specific activation of NFκB in the developing pulmonary vasculature remain unknown.

The tissue microenvironment modulates angiogenesis in development and disease. During early lung development, the alveolar epithelium regulates vascular patterning by expressing VEGF to promote EC survival, proliferation, and migration. In cancer, activated stromal fibroblasts develop a myofibroblast phenotype, co-localize with tumor vasculature, and promotes

AJRCMB Articles in Press. Published December 02, 2020 as 10.1165/rcmb.2020-0153OC
Copyright © 2020 by the American Thoracic Society

angiogenesis by expressing growth factors and modulating the extracellular matrix (7). Although myofibroblasts are required for alveolarization (8), whether they function to regulate pulmonary angiogenesis has not been explored.

In this study, we hypothesized that unique factors in the early alveolar microenvironment induce temporal-specific activation of NFκB in the pulmonary endothelium. We profiled the lung secretome during development and identified transforming growth factor beta-induced protein (TGFBI) as protein highly expressed by myofibroblasts during early alveolarization. We show that TGFBI induces NFκB activation through αvβ3 integrins, increasing nitric oxide (NO) production by increasing the expression of colony stimulating factor-3 (*Csf3*), an NFκB downstream target gene. *Tgfbi* null mice exhibit decreased pulmonary vascular density, and a marked impairment of alveolar and vascular growth in repose to chronic hyperoxia. Further, TGFBI expression was dysregulated in a premature lamb model of disrupted alveolarization. Together, our data identify a novel myofibroblast-endothelial cell axis that serves to guide pulmonary angiogenesis during early alveolarization and implicate a role for dysregulated TGFBI in the pathogenesis of BPD.

Methods: Please see the Online Methods for full details.

Animal Models

C57BL/6 neonatal mice at early alveolarization (P6) and adult mice were purchased from Charles River Lab. *Tgfbi* null (*Tgfbi*$^{-/-}$) mice have been described previously (9). Mice containing an endothelial cell specific deletion of *Ikkβ* were generated by crossing *Ikkβ*$^{fl/fl}$ mice (10) with *Pdgfb-iCre* mice (11). For hyperoxia experiments, litters of P0 pups were maintained in room air

AJRCMB Articles in Press. Published December 02, 2020 as 10.1165/rcmb.2020-0153OC
Copyright © 2020 by the American Thoracic Society

(normoxia) or 80% O_2 (hyperoxia) for 14 days (12). Lung morphometric analysis was performed as previously described (6, 13).

The methods for delivery and management of chronically ventilating preterm lambs are reported (14-17). Time-pregnant ewes at 132 ± 2 d of gestation (term ~150 d gestation) were used. At ~3h of age, the preterm lambs were randomized to invasive mechanical ventilation (IMV) or noninvasive respiratory support (NRS), as previously described (16) for a total of 21d. Control lambs were born at term.

Protocols for the animal studies adhered to American Physiological Society/US National Institutes of Health guidelines for humane use of animals for research and were prospectively approved by the Institutional Animal Care and Use Committee at Stanford University and the University of Utah Health Sciences Center.

Lung Conditioned Media

Lung conditioned media (LCM) was prepared from lung tissue from C5BL/6 mice at the early alveolar (P6), late alveolar (P16) and adult (8-10 weeks) stages of development (18), and proteins analyzed by 2D DIGE protein expression profiling.

Western Immunoblot and Immunofluorescence

Whole cell protein lysates were extracted from lung tissue and western blot performed (13). Immunostaining was performed on formalin-fixed or frozen lung sections (6), probed with primary antibodies against CD31, TGFBI, NFκB p65 or von Willebrand factor.

Isolation of Primary Pulmonary Endothelial Cells (PEC)

AJRCMB Articles in Press. Published December 02, 2020 as 10.1165/rcmb.2020-0153OC
Copyright © 2020 by the American Thoracic Society

PEC were isolated from P6 or adult C57BL/6, *Tgfbi*$^{-/-}$and *Tgfbi*$^{+/+,}$ *Pdgfb*-iCre$^{-/-}$*Ikkβ*$^{fl/fl}$ and *Pdgfb*-iCre$^{+/-}$*Ikkβ*$^{fl/fl}$ mice as described previously (6, 13). PEC isolation by this method with CD31 magnetic beads were approximately 95% pure based on staining for additional EC markers such as CD102 (8). Cells from passage 0-2 were used for all assays as described in the Supplemental Methods. TGFBI neutralization was performed with anti-TGFBI antibodies (4 μg/ml), TGFBI stimulation with recombinant TGFBI (10 μg/ml) (19). NFκB inhibition with the pharmacologic inhibitor, BAY11-0782 (2.5 μM), and αvβ3 inhibition with signaling anti-αvβ3 integrin (4 μg/ml) antibodies.

RNA interference

PEC were transfected with non-targeting control (NTC) , integrin αV, integrin β3, or Csf3 On-Target Plus SMART pool siRNA using Lipofectamine 2000 for 6h as previously described (20).

Multiplex Fluorescent In Situ Hybridization (ISH)

PEC from P6 *Pdgfb-Cre*$^{+}$*Ikkβ*$^{fl/fl}$ and *Pdgfb-Cre*$^{-}$*Ikkβ*$^{fl/fl}$ mice were treated with 4-OHT and stimulated with TGFBI, colocalization of *Csf3* and PEC marker *Pecam1* were detected in PEC using RNAscope ISH per the manufacturer's protocol (ACD).

RNA-Seq Analysis

Total RNA was extracted and RNA-sequencing performed by Quick Biology. Genes showing altered expression with $P< 0.05$ and more than 1.5-fold change were considered differentially expressed.

AJRCMB Articles in Press. Published December 02, 2020 as 10.1165/rcmb.2020-0153OC
Copyright © 2020 by the American Thoracic Society

Measurement of NO in PEC

NO production was determined by loading the cells with 4-amino-5-methylamino-2',7'-difluorofluorescein diacetate (DAF-FM) prior to immunofluorescent imaging as previously described (21).

Statistics

Statistical differences between two groups were determined by Student's t-test, One- or Two-Way ANOVA as appropriate. A P value of ≤0.05 was considered statistically significant.

Results:

Factors secreted by the early alveolar lung activate pro-angiogenic pathways in adult PEC.

To determine if factors present in the early alveolar microenvironment activate NFκB and modulate PEC angiogenic function, we collected lung conditioned media (LCM) from mice at different stages of development and assessed NFκB activation and PEC migration. Under control conditions, NFκB subunits are constitutively expressed, but only translocate to the nucleus upon activation. At baseline, adult PEC demonstrated minimal active NFκB (Fig. 1A). However, incubation with early alveolar LCM increased NFκB activation by 2.65-fold ($P<0.001$) (Fig. 1A and B). In contrast, incubation with late alveolar LCM increased NFκB activation only slightly ($P<0.05$), and adult LCM had no effect. Similarly, adult PEC migrated slowly when cultured in starvation media (Fig. 1C). The early alveolar LCM was as effective as 5% FBS in inducing adult PEC migration, resulting in 43% scratch closure ($P<0.0001$). In contrast, the adult LCM induced migration only minimally ($P<0.05$). Taken together, these data suggested that factors present in

AJRCMB Articles in Press. Published December 02, 2020 as 10.1165/rcmb.2020-0153OC
Copyright © 2020 by the American Thoracic Society

the early alveolar lung microenvironment can induce NFκB activation and promote migration in adult PEC.

TGFBI is highly expressed in the early alveolar lung but absent in the adult lung.

To identify factors uniquely present in the early alveolar lung microenvironment, we compared all of the secreted proteins in the three LCM by two-dimensional difference gel electrophoresis (2-D DIGE) (Fig. E1), and identified 20 proteins that were highly expressed in the early alveolar lung secretome by mass spectrometry (Table E1). Of this group we selected transforming growth factor induced protein (TGFBI) for further investigation, a classically secreted protein that has recently been shown to be highly expressed by myofibroblasts by single cell RNA sequencing of the developing mouse lung (22). We confirmed higher expression of TGFBI in the early alveolar LCM ($P<0.001$, Fig.2 A), and in agreement with previous data (9), highest TGFBI protein in whole lung during early alveolarization, followed by an age-dependent decrease over time (Fig. 2B). Immunostaining of early alveolar lung tissue identified numerous cells with intense TGFBI expression (Fig. 2C), located at the tips of secondary septa, characteristic locations for alveolar myofibroblasts. In contrast, TGFBI immunoreactivity was completely absent in the adult lung. Similar findings were observed in the lungs of lambs (Fig. 2D), with high TGFBI expression in cells at the septal tips at 1 day of life, corresponding to early alveolarization, but reduced TGFBI expression by three weeks of age.

TGFBI is necessary and sufficient for promoting early alveolar and adult PEC migration.

We next determined whether TGFBI was required for the early alveolar LCM to enhance adult PEC migration. The addition of anti-TGFBI antibodies, but not isotype control IgG, significantly impaired, but did not completely abrogate, the capacity of the early alveolar LCM to

AJRCMB Articles in Press. Published December 02, 2020 as 10.1165/rcmb.2020-0153OC
Copyright © 2020 by the American Thoracic Society

promote adult PEC migration (P<0.0001, Fig.3A), but had no effect on its proliferative effect (Fig. 3B). To determine whether TGFBI was sufficient to promote PEC migration, we employed recombinant TGFBI (rTGFBI) in microfluidic chemotaxis assays that permitted the creation of stable, linear gradients of chemotactic agents. Early alveolar PEC exposed to a gradient of starvation media migrated randomly, while those exposed to a gradient of VEGF demonstrated directed migration toward the source (P<0.0001) (Fig. 3C). Both the early alveolar LCM and rTGFBI induced similar directed migration, although VEGF was a more potent chemoattractant as it was able to stimulate migration at much lower doses. Moreover, rTGFBI promoted migration of both the early alveolar and adult PEC in endothelial scratch assays and Boyden chamber assays (Fig. E2).

TGFBI-mediated PEC migration is NFκB-dependent.

We next assessed whether the pro-migratory effect of TGFBI is NFκB-dependent. Similar to the migration results, early alveolar LCM containing control IgG increased NFκB activation by 80% (P<0.001), but the addition of anti-TGFBI antibodies significantly blunted this effect (P<0.05) (Fig. 4A). rTGFBI significantly increased NFκB activity in early alveolar PEC (Fig. 4B, P<0.001), and increased NFκB-DNA binding as early as 30 min, with peak NFκB-DNA binding observed at 1h (Fig. 4C). In addition, inhibiting NFκB with BAY-7082 (23), completely abrogated TGBFI-mediated migration (P<0.0001, Fig. 4D). Further, we performed studies using PEC obtained from mice containing an endothelial-specific deletion of *IKKβ*, the primary activator of NFκB in early alveolar PEC (20). Although rTGFBI increased migration in WT PEC (P<0.01), TGFBI-induced migration was absent in PEC lacking *IKKβ*. Taken together, these data demonstrate that TGFBI-mediated migration is IKKβ/NFκB dependent (Fig. 4E).

AJRCMB Articles in Press. Published December 02, 2020 as 10.1165/rcmb.2020-0153OC
Copyright © 2020 by the American Thoracic Society

TGFBI–mediated NFκB activation and endothelial migration requires avβ3 integrins.

We next performed studies to identify how TGFBI was mediating these effects. TGFBI contains a carboxy-terminal Arg-Gly-Asp (RGD) sequence that allows binding to integrins (24). We focused initially on αvβ3, an integrin up-regulated in angiogenic vascular tissue (25), that activates NFκB in EC (26, 27). rTGFBI significantly increased NFκB activity in early alveolar PEC pre-treated with control IgG but had no effect on PEC treated with anti-αvβ3 integrin antibodies (Fig. 5A and B). Although both rTGFBI alone and rTGFBI+IgG promoted PEC migration to a similar degree (Fig. 5C), anti-αvβ3 antibodies completely blocked rTGFBI-induced PEC migration. Finally, we transfected early alveolar PEC with NTC, αv integrin, or β3 integrin siRNA. In vehicle-stimulated cells, migration was similar between the three groups (Fig. 5D). rTGFBI significantly increased migration in the NTC-transfected PEC ($P<0.01$) but did not increase migration in PEC transfected with either αv or β3 siRNA.

TGFBI promotes migration of early alveolar PEC by increasing NFκB-mediated Csf3 expression to enhance NO production.

To identify mechanism by which TGFBI promotes PEC migration, we profiled TGFBI-responsive genes using RNA-Seq. Given that rTGFBI stimulated both early alveolar and adult PEC migration (Fig. E2), we looked for genes induced by rTGFBI in both groups. Hierarchical clustering of differentially expressed genes demonstrated good clustering of vehicle- and rTGFBI-stimulated samples (Fig. 6A). rTGFBI significantly dysregulated 56 genes in early alveolar (Table E2) and 64 genes in adult PEC (Table E3), however, only 3 genes were shared (Fig. E3A). Colony stimulating factor-3 (*Csf3),* a known NFκB- target gene, was among the shared genes, upregulated 3.01-fold in early alveolar and 2.77-fold in adult PEC by rTGFBI (Fig. E3B). We confirmed that

AJRCMB Articles in Press. Published December 02, 2020 as 10.1165/rcmb.2020-0153OC
Copyright © 2020 by the American Thoracic Society

rTGFBI induced a 3.4-fold increase in *Csf3* gene expression in early alveolar PEC ($P<0.05$) by qPCR (Fig. 6B), and increased CSF3 protein ($P<0.01$) (Fig. 6C). To determine if *Csf3* expression in the PEC requires NFκB activation, we performed multiplex *in situ* hybridization to simultaneously detect *Csf3* and *Pecam1* in $Ikk\beta^{+/+}$ and $Ikk\beta^{-/-}$ PEC isolated from P6 pups. Using this method, we conformed that *Csf3* is expressed in *Pecam1* positive cells (Fig.6D). rTGFBI stimulation for 4h increased *Csf3* expression by 2.7-fold in $Ikk\beta^{+/+}$ PEC ($P<0.0001$), but failed to increase *Csf3* expression in the $Ikk\beta^{-/-}$ PEC (Fig. 6D).

Prior studies found that CSF3 promotes EC migration by increasing in NO (28). Therefore, we next loaded cells with the NO sensitive dye, DAF-FM diacetate prior to stimulation with vehicle or rTGFBI and found that rTGFBI increased NO in the PEC by more than 2-fold compared to vehicle at 4 and 24h. (Fig. 6E, E3D). To determine if the TGFBI-mediated effects require *Csf3*, we performed additional studies where we silenced *Csf3*. Transfection of early alveolar PEC with *Csf3* siRNA effectively reduced CSF3 protein expression by 42h (Fig. E3C). Incubation of NTC siRNA-transfected cells with rTGFBI for 8h increased migration 2-fold ($P< 0.0001$) (Fig. 6F), but did not significantly enhance migration in *Csf3* siRNA-transfected cells. rTGFBI also enhanced NO production in NTC siRNA-transfected cells (Fig. 6G). However, rTGFBI-mediated increases in NO were significantly decreased with *Csf3* silencing. Taken together, these results demonstrate that TGFBI promotes PEC migration by augmenting NFκB-mediated *Csf3* expression to increase NO production.

AJRCMB Articles in Press. Published December 02, 2020 as 10.1165/rcmb.2020-0153OC
Copyright © 2020 by the American Thoracic Society

Loss of TGFBI impairs pulmonary vascular growth in mice, and TGFBI expression is dysregulated in preterm lambs with impaired alveolarization.

To assess the physiological role of TGFBI in alveolarization and pulmonary angiogenesis, we evaluated mice containing a global deletion of TGFBI in normoxia and in response to chronic hyperoxia, a stimulus that disrupts pulmonary angiogenesis and alveolarization (29). These mice were reported to have impaired alveolarization at baseline, but abnormalities in vascular growth were not observed in that initial report. In keeping with prior results, *Tgfbi* null mice exhibited a 20% decrease in radial alveolar count ($P<0.0001$) and a 128% increase in distal airspace area ($P<0.0001$) compared to WT mice (Fig. 7A-C). As expected, chronic hyperoxia disrupted alveolarization in the WT mice, but induced a more exaggerated phenotype in the *Tgfbi* null mice, reducing radial alveolar count by almost 70% ($P<0.0001$) and further increased the already dilated distal airspaces ($P<0.001$). Under control conditions, *Tgfbi* null mice exhibited a 33% reduction in pulmonary vascular density as compared to WT ($P<0.0001$) (Fig. 7D and E). Chronic hyperoxia reduced pulmonary vascular density in WT mice by 46% ($P<0.0001$), but caused a more exaggerated disruption of pulmonary vascular growth in the *Tgfbi* null mice, decreasing pulmonary vascular density by 70% ($P<0.0001$), resulting in an almost 3-fold reduction in distal vessels in *Tgfbi* null compared to WT mice. Taken together, these results demonstrate that TGFBI is required for physiologic pulmonary vascular growth, and that loss of TGFBI worsens the detrimental effects of chronic hyperoxia on alveolarization and angiogenesis.

Finally, we explored whether TGFBI expression was altered in a large animal model of BPD, where preterm lambs are supported with either non-invasive respiratory support (NRS) or invasive mechanical ventilation (IMV). Control, term lambs had focal staining of TGFBI throughout the lung, including high expression at the tips of all the secondary septa (Fig. 7F,

AJRCMB Articles in Press. Published December 02, 2020 as 10.1165/rcmb.2020-0153OC
Copyright © 2020 by the American Thoracic Society

arrows). Preterm lambs supported with NRS exhibited many, thin secondary septa, and a marked reduction in TGFBI immunostaining. Preterm lambs supported by IMV, however, had abnormally thickened secondary septa, with a heightened expression but abnormal localization of TGFBI along the length of the thick secondary septa rather than the normal localization at the septal tips.

Discussion:

During early postnatal life, growth of the pulmonary vasculature serves as a driver of alveolarization. In this study, we explored the mechanisms that activate pro-angiogenic NFκB signaling in the pulmonary endothelium during early alveolarization. We identified TGFBI, as a secreted protein highly expressed by myofibroblasts in early alveolarization (22), corresponding to the time when NFκB is endogenously active in the pulmonary vasculature (6). We show that TGFBI activates NFκB in PEC and enhances NFκB-mediated EC migration via αvβ3 integrins. We further show that TGFBI stimulation increases *Csf3* expression, serving to enhance NO production. Finally, we demonstrate that loss of TGFBI in mice impairs pulmonary vascular development at baseline and severely impairs alveolar and vascular growth in chronic hyperoxia, and that TGFBI expression and localization is aberrant in a preterm lamb model of disrupted alveolarization. In summary, our studies identify a novel axis, whereby developmental expression of TGFBI activates NFκB and promotes pulmonary endothelial angiogenesis during this critical window of vascular development.

Pulmonary angiogenesis is essential for alveolarization, and disrupted angiogenesis contributes to the pathogenesis of bronchopulmonary dysplasia (BPD), the most common complication of premature birth (30). Our lab previously identified the NFκB pathway as an important regulator of pulmonary angiogenesis during alveolarization (6). However, the

AJRCMB Articles in Press. Published December 02, 2020 as 10.1165/rcmb.2020-0153OC
Copyright © 2020 by the American Thoracic Society

mechanisms allowing for temporal-specific activation of pro-angiogenic NFκB signaling in the pulmonary vasculature was not identified. These results highlight the role of paracrine factors secreted from alveolar myofibroblasts in the creation of a pro-angiogenic niche that activates NFκB to support pulmonary vascular growth during early alveolarization.

By profiling developmental differences in the lung microenvironment, we identified TGFBI as a temporally-regulated protein highly expressed during early alveolarization. However, the capacity of the EA-LCM to promote migration and activate NFκB was not completely abrogated by the anti-TGFBI antibodies, suggesting that additional factors present in the early alveolar lung microenvironment also serve to enhance NFκB-dependent pro-angiogenic signaling. TGFBI binds both extracellular matrix (31, 32) and integrins (33-35), suggesting a possible role as a bifunctional linker protein that connects cells to the matrix (31). TGFBI mRNA is biphasically altered in the hyperoxia mouse model of BPD (9) and induced during bleomycin-mediated fibrotic lung injury (36). Importantly, single cell RNA sequencing in the developing murine lung identified TGFBI as a highly discriminating gene for myofibroblasts (22). In our study, TGFBI was expressed at the tips of secondary crests, characteristic locations for myofibroblasts (8), concordant with a prior report that identified high expression of TGFBI in the septal tips of a two year-old child, leading the authors to speculate a putative role in alveolar morphogenesis (37).

In other systems, TGFBI is regulated by TGFβ. TGFβ isoforms play a complex role in lung development. Although TGFβ1 is expressed in the developing lung during branching morphogenesis (38), loss of TGFβ1 does not disrupt lung development (39). However, loss of TGFβ3 induces alveolar hypoplasia and extensive intrapulmonary hemorrhage, suggesting role for TGFβ3 in pulmonary vasculature stabilization (40). Impaired alveolarization is also observed in

AJRCMB Articles in Press. Published December 02, 2020 as 10.1165/rcmb.2020-0153OC
Copyright © 2020 by the American Thoracic Society

mice with global deletions of Smad3, the downstream effector of TGFβ (41). Taken together these data highlight the importance of precise TGFβ signaling in the correct cells at the right time to support lung development. Further studies will be needed to determine if TGFβ is the primary regulator of TGFBI in the early alveolar lung, however, as a putative downstream effector of TGFβ, our data highlight a role for TGFBI in coordinating alveolar and vascular growth during alveolarization.

TGFBI promotes cell adhesion, migration and proliferation of diverse cell types by interacting via integrins (42). We specifically investigated αvβ3 integrins given their established role in angiogenesis. The αvβ3 integrin is highly expressed by newly forming blood vessels (25). Activation of αvβ3 promotes endothelial migration (43), and blocking αvβ3 inhibits tumor angiogenesis (44) and impairs lumen formation and vascular patterning in the embryo (45). Further, αvβ3 activates NFκB to promote EC adhesion, survival, and migration (26, 46). Moreover, TGFBI promotes adhesion and migration of human umbilical EC via αvβ3 (35). Concordant with these studies, we found that TGFBI-stimulated PEC migration was blocked by inhibiting either NFκB or αvβ3. Taken together, our data demonstrate that TGFBI promotes PEC migration via αvβ3 to induce pro-angiogenic NFκB signaling.

We next investigated the downstream mechanisms by which TGFBI promotes PEC migration, using RNA-Seq to identify novel TGFBI-regulated genes. One of the few shared targets in early alveolar and adult PEC was *Csf3* (encoding G-CSF), a known NFκB target gene (47) that promotes endothelial migration (48). GCSF increases the expression and activation of endothelial nitric oxide synthase (eNOS) to augment NO production (28). NO is produced locally at lamellipodia of migrating human EC, and lung EC from *eNOS* null mice migrate more slowly and

AJRCMB Articles in Press. Published December 02, 2020 as 10.1165/rcmb.2020-0153OC
Copyright © 2020 by the American Thoracic Society

display impaired capillary formation (49-51). In our study, TGFBI increased NO production in PEC, and silencing *Csf3* blocked both TGFBI-mediated NO production and PEC migration. Further, rTGFBI failed to induce *Csf3* expression in *Ikkβ*$^{-/-}$ PEC, demonstrating that the TGFBI-mediated *Csf3* upregulation requires NFκB signaling. In preterm lambs, prolonged IMV reduced eNOS protein and pulmonary capillary and microvessel abundance (52, 53). Taken together, these studies identify *Csf3* as a central downstream mechanism for the pro-angiogenic effects of TGFBI.

Finally, as proof of concept for the importance of TGFBI *in vivo*, we performed studies using *Tgfbi* null mice and a preterm lamb model of impaired alveolarization (9, 16). Although a reduction in total vWF positive vessels was not observed in the *Tgfbi* null mice at P7 in the original description of these mice, we found that by P14, there was a reduction in the density of vessels <100 μm in diameter. Further, this vascular phenotype was markedly exaggerated by chronic hyperoxia. We also found that TGFBI expression was reduced in preterm lambs treated with NRS, consistent with delayed alveolarization observed in this group. Importantly, in preterm lambs maintained with the more injurious, IMV strategy, TGFBI expression was abnormally increased along the thickened septal tips, similar to the abnormal accumulation of elastin and mesenchymal cell proliferation reported (14, 54). These studies suggest that both the correct amount and the correct location of TGFBI is required to optimally support vascular growth. Further, these preclinical studies support recent clinical studies that offer additional evidence of the importance of TGFBI in the developing human lung. In a study of 50 twin pairs affected and unaffected with BPD, rare variants in *TGFBI* were associated with an increased risk for BPD (55). In a subsequent, larger study that employed whole exome sequencing in infants with extreme phenotypes of BPD, rare variants in *TGFBI* were again identified in affected but not unaffected subjects (56). Taken together, these studies provide compelling data to highlight the importance of TGFBI in promoting

AJRCMB Articles in Press. Published December 02, 2020 as 10.1165/rcmb.2020-0153OC
Copyright © 2020 by the American Thoracic Society

distal lung development and implicate a role for disrupted TGFBI signaling in the pathogenesis of BPD.

Our study has some limitations. Our proteomic analysis of the LCM utilized two-dimensional difference gel electrophoresis (2D-DIGE), protein spots were manually selected, and only the top 20 differentially expressed proteins identified by mass spectroscopy. Thus, there are likely additional protein present in the LCM that serve to enhance NFκB signaling and modify the pro-angiogenic phenotype of the PEC in addition to TGFBI. Newer methodologies that allow for a broader identification of differentially expressed proteins, including those with low abundance that may not have been identified with 2D-DIGE, represent important future studies. Although we were able to clearly show that TGFBI promotes PEC migration by binding to αvβ3 integrins, it is possible that TGFBI can also bind to addition integrins, resulting in distinct downstream effects. We performed transcriptomic profiling of primary PEC obtained from neonatal and adult mice in order to identify novel, TGFBI-mediated target genes. Although this approach allowed us to directly compare genes expressed by PEC at two distinct stages in development, there remains the possibility for confounding effects and change in phenotype as a result of cell culture. We attempted to mitigate these confounders by performing the analyses on two separate isolations of cells, and only including genes differentially expressed in both separate isolations. Nevertheless, future studies utilizing single cell RNA-sequencing in the WT and *Tgfbi* null mice could provide a more comprehensive assessment of all of the differentially expressed genes in both the EC and other lung cell types.

In summary, our data identify a paracrine mechanism by which myofibroblast expression of TGFBI promotes pulmonary angiogenesis through an αvβ3/NFκB axis that increases CSF3-

AJRCMB Articles in Press. Published December 02, 2020 as 10.1165/rcmb.2020-0153OC
Copyright © 2020 by the American Thoracic Society

mediated NO production. Given the ability of TGFBI to bind extracellular matrix components highly expressed in the developing lung, local secretion of TGFBI by myofibroblasts may serve to create an angiogenic niche that promotes pulmonary vascular growth along the developing septa. Taken together, our studies identify a novel pathway allowing for myofibroblast-endothelial cross talk, and we speculate that TGFBI dysregulation may contribute to the aberrant pulmonary angiogenesis observe in the setting of impaired alveolarization.

Acknowledgements: None.

AJRCMB Articles in Press. Published December 02, 2020 as 10.1165/rcmb.2020-0153OC
Copyright © 2020 by the American Thoracic Society

Figure Legends:

Figure 1: Factors secreted by the early alveolar lung activate pro-angiogenic pathways in adult pulmonary endothelial cells. (A) Representative immunofluorescent images of adult PEC incubated with starvation media, or early alveolar (EA), late alveolar (LA) or adult lung conditioned media (LCM) for 24h followed by immunostaining to detect the NFκB subunit, p65 (red) and chromatin (blue). (B) Quantification of the total intensity of nuclear p65 with *P<0.05, and ****P<0.0001 vs. starvation, and ####P<0.0001 vs. EA-LCM, with n=6 per group. (C) EC scratch assays performed using adult PEC incubated with starvation media, 5% FBS, EA-LCM, and adult LCM, and the percent scratch area covered at 24h calculated. ****P<0.0001 vs. starvation, and ####P<0.0001 vs. EA-LCM, with n=3 per group.

Figure 2: TGFBI is highly expressed in the early alveolar lung but absent in the adult lung.

(A) Western blot to determine TGFBI protein in the EA-, LA-, and adult LCM. ****P<0.0001 vs. EA=LCM, with n=3. (B) Western blot to determine TGFBI protein relative to β-actin in whole lung from mice at the early alveolar (P6), late alveolar (P16), and adult (P30) stages of development. **P<0.01 and ****P<0.0001 vs. P6, and #P<0.05 vs. P16, with n=4 per group. (C) Representative images obtained from lung cryosections obtained from P6 and adult mice to detect CD31 (green), TGFBI (red) and chromatin (blue). Arrows point to TGFBI-positive cells at tips of secondary septa. Calibration mark=100μm. (D) Representative images obtained from lung tissue from lambs at the early alveolar (Day 1) and late alveolar (3 week) stages of development to detect α-smooth muscle-actin (green), TGFBI (red) and chromatin (blue). Calibration mark=50μm.

AJRCMB Articles in Press. Published December 02, 2020 as 10.1165/rcmb.2020-0153OC
Copyright © 2020 by the American Thoracic Society

Figure 3: TGFBI is necessary and sufficient to promote PEC migration. (A) Endothelial scratch assays were performed using adult PEC incubated with starvation media, 5% FBS, EA-LCM, EA-LCM plus isotype control IgG, and EA-LCM plus anti-TGFBI antibodies (4 μg/ml) and the percent scratch area covered at 24h calculated. ****P<0.0001 vs. starvation, and ####P<0.0001 vs. EA-LCM, with n=3 per group. Representative results from three separate experiments. (B) BrdU incorporation assays to assess adult PEC proliferation at 24h in cells incubated with 5% FBS, EA-LCM, EA-LCM + IgG, and EA-LCM + anti-TGFBI antibodies. ****P<0.0001 vs. starvation with n=3-6 per group. (C) Tracks of individual cells (top) and directional histograms (bottom) from live cell imaging and tracking of early alveolar PEC subjected to microfluidic chemotaxis assays performed with starvation media, EA-LCM, starvation +TGFBI or starvation + VEGF (50 ng/ml) with each chamber containing a source on the right side and a sink on the left. Total number of individual cells tracked is reported in the upper left corner, and the number of cells migrating away (black) or toward (red) in the bottom left and right corners respectively. In each group there were between 3-5 cells with a migration of net zero, accounting for the remaining cells making up the total n number. P value is shown on the image.

Figure 4: TGFBI-mediated pulmonary endothelial cell migration is NFκB-dependent. (A) Representative images of adult PEC incubated with starvation media, EA-LCM + IgG, and EA-LCM + anti-TGFBI antibodies for 24h followed by immunostaining to detect p65 (red) and chromatin (blue), with quantification to determine the total intensity of nuclear p65 over nuclear area. *P<0.05, and ***P<0.001 vs. starvation, and #P<0.05 vs. EA-LCM + IgG, with n=5 per group. (B) Representative images from early alveolar PEC incubated with starvation media + vehicle or starvation media + rTGFBI for 24h stained to detect the p65 (red), CD31(green), and

AJRCMB Articles in Press. Published December 02, 2020 as 10.1165/rcmb.2020-0153OC
Copyright © 2020 by the American Thoracic Society

DAPI (blue), with quantification of total intensity of nuclear p65. ****P<0.0001 with n=127 control cells and n=112 rTGFBI-stimulated cells. (C) Representative EMSA to detect NFκB-DNA binding in early alveolar PEC exposed to starvation media, or starvation media + TGFBI. (D) Scratch assays using early alveolar PEC stimulated with starvation media, starvation media + rTGFBI, or starvation media +rTGFBI and BAY 11-7082 (2.5 μM), with the percent scratch area covered at 24h calculated. ***P<0.001 vs. starvation and ####P<0.0001 vs. rTGFBI, with n=4 per group. (E) Scratch assays performed using wild type PEC (*Ikkβ* $^{+/+}$) and PEC lacking the NFκB activator, IKKβ (*Ikkβ* $^{-/-}$) stimulated with starvation media, EGM, starvation media + rTGFBI and the percent scratch area covered at 24h calculated. **P<0.01 and ****P<0.0001 vs. starvation and ##P<0.01 vs. TGFBI treated *Ikkβ* $^{+/+}$ PEC, with n=4 per group.

Figure 5: TGFBI–mediated endothelial migration requires αvβ3 integrins. (A) Representative images obtained from early alveolar PEC pretreated with either IgG or anti-αvβ3 antibodies prior to stimulation with starvation media + vehicle or starvation media + rTGFBI for 24h stained to detect the p65 (red), CD31(green), and DAPI (blue), with (B) quantification of total intensity of nuclear p65. **P<0.01 versus starvation + IgG, and ## versus rTGFBI + IgG with n=4. (C) Scratch assays with early alveolar PEC incubated with starvation media, EGM, starvation media + rTGFBI, starvation media + rTGFBI + IgG, and starvation media + rTGFBI plus anti-αvβ3 antibodies and the percent scratch area covered at 24h calculated. *P<0.05 and ***P<0.001 vs. starvation and ##P<0.01 vs. starvation + rTGFBI+ IgG, with n=3 per group. Representative result from 2 independent experiments. (D) Scratch assays were performed using early alveolar PEC transfected with NTC, integrin αv, and integrin β3 siRNA. At 48h post transfection, the groups were incubated with starvation media, EGM, starvation media + rTGFBI and the percent scratch

AJRCMB Articles in Press. Published December 02, 2020 as 10.1165/rcmb.2020-0153OC
Copyright © 2020 by the American Thoracic Society

area covered at 24h calculated. **P<0.01 vs. starvation, and #P<0.05 and ##P<0.01 vs. NTC stimulated with rTGFBI, with n=3-4 per group. Representative result from 4 independent experiments.

Figure 6: TGFBI induces an NFκB-dependent expression of Csf3, a modulator of nitric oxide, in early alveolar PEC. (A) Heat map of differentially expressed genes identified by RNA-Seq in early alveolar and adult PEC stimulated with vehicle or rTGFBI for 6h. Up-regulated genes are in red and down-regulated genes in green. (B) Gene expression of *Csf3* was determined by qRT-PCR in early alveolar PEC stimulated with vehicle or rTGFBI for 6h. *P<0.05 vs. vehicle with n=4 per group. (C) Representative western blot to detect CSF3 protein expression in whole cell lysates obtained from early alveolar PEC stimulated with vehicle or rTGFBI for 4hr. (D) Representative *in situ* hybridization images to detect *Csf3* (red) and *Pecam1* (green) in $Ikk\beta^{+/+}$ and $Ikk\beta^{-/-}$ PEC treated with vehicle or rTGFBI for 4h, with quantification of the fold change in raw integrated density of *Csf3* mRNA particles per cell compared to vehicle. *** P=0.0006 vs. $Ikk\beta^{+/+}$ PEC. (E) NO production assays in early alveolar PEC stimulated with starvation media containing vehicle or rTGFBI for 4hr and loaded with the NO sensitive dye, DAF-FM. Representative images taken to detect NO (green) and chromatin (blue). Calibration mark=100µm. Quantification of the raw integrated density of NO fluorescent signal per cell in early alveolar PEC stimulated with vehicle or rTGFBI for 4h, with **P<0.01 vs. vehicle, with n=5-8 per group. Results are representative of 3 independent experiments. (F) Boyden chamber assays to detect chemotactic migration in early alveolar PEC transfected with NTC or Csf3 siRNA incubated at 48h after transfection with starvation media or starvation media containing rTGFBI for 8h. ****P <0.0001 vs. vehicle and ##P<0.01 vs. NTC siRNA transfected PEC treated with rTGFBI, with n=10-12 replicates. Results are a representative example of three independent experiments. (G) NO

AJRCMB Articles in Press. Published December 02, 2020 as 10.1165/rcmb.2020-0153OC
Copyright © 2020 by the American Thoracic Society

production assays in early alveolar PEC transfected with NTC or Csf3 siRNA and stimulated with vehicle or rTGFBI for 4h. Representative images to detect NO (green) and chromatin (blue). Quantification of the fold change in raw integrated density of NO fluorescence per cell in NTC and Csf3 siRNA transfected PEC stimulated with rTGFBI compared to vehicle for 4h. ***P=0.0008 vs. NTC transfected PEC.

Figure 7. Loss of TGFBI in mice impairs pulmonary parenchymal and vascular growth and TGFBI expression is dysregulated in experimental models of impaired alveolarization. (A) Representative images obtained from P14 wild type (WT) and *Tgfbi* null mice maintained in normoxia or chronic hyperoxia (80% O2 from P1-P14). Calibration bar=100μm. Quantification of radial alveolar counts (B) and (C) distal airspace area. **P<0.01 and ****P<0.0001 vs. normoxia for each genotype, and ###P<0.001 and ####P<0.0001 vs. WT via 2-WAY ANOVA, with n=4-7 per group. The asterisk (*) denote differences between normoxia and hyperoxia for each genotype, and that the hashtags (#) denote differences between the genotypes in each condition. (D) Representative images stained to detect vWF (red) and DAPI (blue) in lungs taken from mice at P14. Calibration bar=100μm. (E) Quantification of vWF-stained vessels less than 100μm per high powered field in 20 non-overlapping sections per mouse. ****P>0.0001 vs. normoxia for each genotype, and ####P<0.0001 vs. WT with n=5-7 mice per group. (F) Representative images obtained from control term newborn lambs, and premature lambs treated with noninvasive respiratory support (NRS) or invasive mechanical ventilation (IMV), stained to detect TGFBI (red), alpha-smooth muscle actin (green) and chromatin (blue). Calibration bar=20 μm.

AJRCMB Articles in Press. Published December 02, 2020 as 10.1165/rcmb.2020-0153OC
Copyright © 2020 by the American Thoracic Society

References:

1. Bourbon J, Boucherat O, Chailley-Heu B, and Delacourt C. Control mechanisms of lung alveolar development and their disorders in bronchopulmonary dysplasia. *Pediatr Res.* 2005;57(5 Pt 2):38R-46R.

2. Jakkula M, Le Cras TD, Gebb S, Hirth KP, Tuder RM, Voelkel NF, et al. Inhibition of angiogenesis decreases alveolarization in the developing rat lung. *Am J Physiol Lung Cell Mol Physiol.* 2000;279(3):L600-7.

3. Thébaud B, Ladha F, Michelakis ED, Sawicka M, Thurston G, Eaton F, et al. Vascular endothelial growth factor gene therapy increases survival, promotes lung angiogenesis, and prevents alveolar damage in hyperoxia-induced lung injury: evidence that angiogenesis participates in alveolarization. *Circulation.* 2005;112(16):2477-86.

4. Islam JY, Keller RL, Aschner JL, Hartert TV, and Moore PE. Understanding the Short- and Long-Term Respiratory Outcomes of Prematurity and Bronchopulmonary Dysplasia. *Am J Respir Crit Care Med.* 2015;192(2):134-56.

5. Baker CD, and Alvira CM. Disrupted lung development and bronchopulmonary dysplasia: opportunities for lung repair and regeneration. *Curr Opin Pediatr.* 2014;26(3):306-14.

6. Iosef C, Alastalo TP, Hou Y, Chen C, Adams ES, Lyu SC, et al. Inhibiting NF-kappaB in the developing lung disrupts angiogenesis and alveolarization. *Am J Physiol Lung Cell Mol Physiol.* 2012;302(10):L1023-36.

AJRCMB Articles in Press. Published December 02, 2020 as 10.1165/rcmb.2020-0153OC
Copyright © 2020 by the American Thoracic Society

7. De Palma M, Biziato D, and Petrova TV. Microenvironmental regulation of tumour angiogenesis. *Nat Rev Cancer.* 2017;17(8):457-74.

8. Bostrom H, Willetts K, Pekny M, Leveen P, Lindahl P, Hedstrand H, et al. PDGF-A signaling is a critical event in lung alveolar myofibroblast development and alveogenesis. *Cell.* 1996;85(6):863-73.

9. Ahlfeld SK, Wang J, Gao Y, Snider P, and Conway SJ. Initial Suppression of Transforming Growth Factor-beta Signaling and Loss of TGFBI Causes Early Alveolar Structural Defects Resulting in Bronchopulmonary Dysplasia. *Am J Pathol.* 2016;186(4):777-93.

10. Li ZW, Omori SA, Labuda T, Karin M, and Rickert RC. IKK beta is required for peripheral B cell survival and proliferation. *J Immunol.* 2003;170(9):4630-7.

11. Claxton S, Kostourou V, Jadeja S, Chambon P, Hodivala-Dilke K, and Fruttiger M. Efficient, inducible Cre-recombinase activation in vascular endothelium. *Genesis.* 2008;46(2):74-80.

12. Hilgendorff A, Reiss I, Ehrhardt H, Eickelberg O, and Alvira CM. Chronic lung disease in the preterm infant. Lessons learned from animal models. *Am J Respir Cell Mol Biol.* 2014;50(2):233-45.

13. Hou Y, Liu M, Husted C, Chen C, Thiagarajan K, Johns JL, et al. Activation of the nuclear factor-kappaB pathway during postnatal lung inflammation preserves alveolarization by suppressing macrophage inflammatory protein-2. *Am J Physiol Lung Cell Mol Physiol.* 2015;309(6):L593-604.

AJRCMB Articles in Press. Published December 02, 2020 as 10.1165/rcmb.2020-0153OC
Copyright © 2020 by the American Thoracic Society

14. Reyburn B, Li M, Metcalfe DB, Kroll NJ, Alvord J, Wint A, et al. Nasal ventilation alters mesenchymal cell turnover and improves alveolarization in preterm lambs. *Am J Respir Crit Care Med.* 2008;178(4):407-18.

15. Albertine KH, Dahl MJ, Gonzales LW, Wang ZM, Metcalfe D, Hyde DM, et al. Chronic lung disease in preterm lambs: effect of daily vitamin A treatment on alveolarization. *Am J Physiol Lung Cell Mol Physiol.* 2010;299(1):L59-72.

16. Null DM, Alvord J, Leavitt W, Wint A, Dahl MJ, Presson AP, et al. High-frequency nasal ventilation for 21 d maintains gas exchange with lower respiratory pressures and promotes alveolarization in preterm lambs. *Pediatr Res.* 2014;75(4):507-16.

17. Joss-Moore LA, Hagen-Lillevik SJ, Yost C, Jewell J, Wilkinson RD, Bowen S, et al. Alveolar formation is dysregulated by restricted nutrition but not excess sedation in preterm lambs managed by noninvasive support. *Pediatr Res.* 2016;80(5):719-28.

18. Chu JE, Xia Y, Chin-Yee B, Goodale D, Croker AK, and Allan AL. Lung-derived factors mediate breast cancer cell migration through CD44 receptor-ligand interactions in a novel ex vivo system for analysis of organ-specific soluble proteins. *Neoplasia.* 2014;16(2):180-91.

19. Park SW, Bae JS, Kim KS, Park SH, Lee BH, Choi JY, et al. Beta ig-h3 promotes renal proximal tubular epithelial cell adhesion, migration and proliferation through the interaction with alpha3beta1 integrin. *Exp Mol Med.* 2004;36(3):211-9.

AJRCMB Articles in Press. Published December 02, 2020 as 10.1165/rcmb.2020-0153OC
Copyright © 2020 by the American Thoracic Society

20. Iosef C, Liu M, Ying L, Rao SP, Concepcion KR, Chan WK, et al. Distinct roles for IkappaB kinases alpha and beta in regulating pulmonary endothelial angiogenic function during late lung development. *J Cell Mol Med.* 2018;22(9):4410-22.

21. Rathel TR, Leikert JJ, Vollmar AM, and Dirsch VM. Application of 4,5-diaminofluorescein to reliably measure nitric oxide released from endothelial cells in vitro. *Biol Proced Online.* 2003;5:136-42.

22. Guo M, Du Y, Gokey JJ, Ray S, Bell SM, Adam M, et al. Single cell RNA analysis identifies cellular heterogeneity and adaptive responses of the lung at birth. *Nat Commun.* 2019;10(1):37.

23. Pierce JW, Schoenleber R, Jesmok G, Best J, Moore SA, Collins T, et al. Novel inhibitors of cytokine-induced IkappaBalpha phosphorylation and endothelial cell adhesion molecule expression show anti-inflammatory effects in vivo. *J Biol Chem.* 1997;272(34):21096-103.

24. Son HN, Nam JO, Kim S, and Kim IS. Multiple FAS1 domains and the RGD motif of TGFBI act cooperatively to bind alphavbeta3 integrin, leading to anti-angiogenic and anti-tumor effects. *Biochim Biophys Acta.* 2013;1833(10):2378-88.

25. Brooks PC, Clark RA, and Cheresh DA. Requirement of vascular integrin alpha v beta 3 for angiogenesis. *Science.* 1994;264(5158):569-71.

26. Scatena M, Almeida M, Chaisson ML, Fausto N, Nicosia RF, and Giachelli CM. NF-kappaB mediates alphavbeta3 integrin-induced endothelial cell survival. *J Cell Biol.* 1998;141(4):1083-93.

AJRCMB Articles in Press. Published December 02, 2020 as 10.1165/rcmb.2020-0153OC
Copyright © 2020 by the American Thoracic Society

27. Bhullar IS, Li YS, Miao H, Zandi E, Kim M, Shyy JY, et al. Fluid shear stress activation of IkappaB kinase is integrin-dependent. *J Biol Chem.* 1998;273(46):30544-9.

28. Ueda K, Takano H, Hasegawa H, Niitsuma Y, Qin Y, Ohtsuka M, et al. Granulocyte colony stimulating factor directly inhibits myocardial ischemia-reperfusion injury through Akt-endothelial NO synthase pathway. *Arterioscler Thromb Vasc Biol.* 2006;26(6):e108-13.

29. Roberts RJ, Weesner KM, and Bucher JR. Oxygen-induced alterations in lung vascular development in the newborn rat. *Pediatr Res.* 1983;17(5):368-75.

30. Bhatt AJ, Pryhuber GS, Huyck H, Watkins RH, Metlay LA, and Maniscalco WM. Disrupted pulmonary vasculature and decreased vascular endothelial growth factor, Flt-1, and TIE-2 in human infants dying with bronchopulmonary dysplasia. *Am J Respir Crit Care Med.* 2001;164(10 Pt 1):1971-80.

31. Billings PC, Whitbeck JC, Adams CS, Abrams WR, Cohen AJ, Engelsberg BN, et al. The transforming growth factor-beta-inducible matrix protein (beta)ig-h3 interacts with fibronectin. *J Biol Chem.* 2002;277(31):28003-9.

32. Hanssen E, Reinboth B, and Gibson MA. Covalent and non-covalent interactions of betaig-h3 with collagen VI. Beta ig-h3 is covalently attached to the amino-terminal region of collagen VI in tissue microfibrils. *J Biol Chem.* 2003;278(27):24334-41.

33. Bae JS, Lee SH, Kim JE, Choi JY, Park RW, Yong Park J, et al. Betaig-h3 supports keratinocyte adhesion, migration, and proliferation through alpha3beta1 integrin. *Biochem Biophys Res Commun.* 2002;294(5):940-8.

AJRCMB Articles in Press. Published December 02, 2020 as 10.1165/rcmb.2020-0153OC
Copyright © 2020 by the American Thoracic Society

34. Kim JE, Jeong HW, Nam JO, Lee BH, Choi JY, Park RW, et al. Identification of motifs in the fasciclin domains of the transforming growth factor-beta-induced matrix protein betaig-h3 that interact with the alphavbeta5 integrin. *J Biol Chem.* 2002;277(48):46159-65.

35. Nam JO, Kim JE, Jeong HW, Lee SJ, Lee BH, Choi JY, et al. Identification of the alphavbeta3 integrin-interacting motif of betaig-h3 and its anti-angiogenic effect. *J Biol Chem.* 2003;278(28):25902-9.

36. Schwanekamp JA, Lorts A, Sargent MA, York AJ, Grimes KM, Fischesser DM, et al. TGFBI functions similar to periostin but is uniquely dispensable during cardiac injury. *PLoS One.* 2017;12(7):e0181945.

37. Billings PC, Herrick DJ, Howard PS, Kucich U, Engelsberg BN, and Rosenbloom J. Expression of betaig-h3 by human bronchial smooth muscle cells: localization To the extracellular matrix and nucleus. *Am J Respir Cell Mol Biol.* 2000;22(3):352-9.

38. Heine UI, Munoz EF, Flanders KC, Roberts AB, and Sporn MB. Colocalization of TGF-beta 1 and collagen I and III, fibronectin and glycosaminoglycans during lung branching morphogenesis. *Development.* 1990;109(1):29-36.

39. Shull MM, Ormsby I, Kier AB, Pawlowski S, Diebold RJ, Yin M, et al. Targeted disruption of the mouse transforming growth factor-beta 1 gene results in multifocal inflammatory disease. *Nature.* 1992;359(6397):693-9.

40. Kaartinen V, Voncken JW, Shuler C, Warburton D, Bu D, Heisterkamp N, et al. Abnormal lung development and cleft palate in mice lacking TGF-beta 3 indicates defects of epithelial-mesenchymal interaction. *Nat Genet.* 1995;11(4):415-21.

AJRCMB Articles in Press. Published December 02, 2020 as 10.1165/rcmb.2020-0153OC
Copyright © 2020 by the American Thoracic Society

41. Chen H, Sun J, Buckley S, Chen C, Warburton D, Wang XF, et al. Abnormal mouse lung alveolarization caused by Smad3 deficiency is a developmental antecedent of centrilobular emphysema. *Am J Physiol Lung Cell Mol Physiol.* 2005;288(4):L683-91.

42. Kim JE, Kim SJ, Lee BH, Park RW, Kim KS, and Kim IS. Identification of motifs for cell adhesion within the repeated domains of transforming growth factor-beta-induced gene, betaig-h3. *J Biol Chem.* 2000;275(40):30907-15.

43. Leavesley DI, Schwartz MA, Rosenfeld M, and Cheresh DA. Integrin beta 1- and beta 3-mediated endothelial cell migration is triggered through distinct signaling mechanisms. *J Cell Biol.* 1993;121(1):163-70.

44. Brooks PC, Montgomery AM, Rosenfeld M, Reisfeld RA, Hu T, Klier G, et al. Integrin alpha v beta 3 antagonists promote tumor regression by inducing apoptosis of angiogenic blood vessels. *Cell.* 1994;79(7):1157-64.

45. Drake CJ, Cheresh DA, and Little CD. An antagonist of integrin alpha v beta 3 prevents maturation of blood vessels during embryonic neovascularization. *J Cell Sci.* 1995;108 (Pt 7):2655-61.

46. Malyankar UM, Scatena M, Suchland KL, Yun TJ, Clark EA, and Giachelli CM. Osteoprotegerin is an alpha vbeta 3-induced, NF-kappa B-dependent survival factor for endothelial cells. *J Biol Chem.* 2000;275(28):20959-62.

47. Dunn SM, Coles LS, Lang RK, Gerondakis S, Vadas MA, and Shannon MF. Requirement for nuclear factor (NF)-kappa B p65 and NF-interleukin-6 binding elements in the tumor

AJRCMB Articles in Press. Published December 02, 2020 as 10.1165/rcmb.2020-0153OC
Copyright © 2020 by the American Thoracic Society

necrosis factor response region of the granulocyte colony-stimulating factor promoter. *Blood.* 1994;83(9):2469-79.

48. Bussolino F, Wang JM, Defilippi P, Turrini F, Sanavio F, Edgell CJ, et al. Granulocyte- and granulocyte-macrophage-colony stimulating factors induce human endothelial cells to migrate and proliferate. *Nature.* 1989;337(6206):471-3.

49. Genis L, Gonzalo P, Tutor AS, Galvez BG, Martinez-Ruiz A, Zaragoza C, et al. Functional interplay between endothelial nitric oxide synthase and membrane type 1 matrix metalloproteinase in migrating endothelial cells. *Blood.* 2007;110(8):2916-23.

50. Lee PC, Salyapongse AN, Bragdon GA, Shears LL, 2nd, Watkins SC, Edington HD, et al. Impaired wound healing and angiogenesis in eNOS-deficient mice. *Am J Physiol.* 1999;277(4):H1600-8.

51. Zhao X, Lu X, and Feng Q. Deficiency in endothelial nitric oxide synthase impairs myocardial angiogenesis. *Am J Physiol Heart Circ Physiol.* 2002;283(6):H2371-8.

52. MacRitchie AN, Albertine KH, Sun J, Lei PS, Jensen SC, Freestone AA, et al. Reduced endothelial nitric oxide synthase in lungs of chronically ventilated preterm lambs. *Am J Physiol Lung Cell Mol Physiol.* 2001;281(4):L1011-20.

53. Bland RD, Albertine KH, Carlton DP, and MacRitchie AJ. Inhaled nitric oxide effects on lung structure and function in chronically ventilated preterm lambs. *Am J Respir Crit Care Med.* 2005;172(7):899-906.

AJRCMB Articles in Press. Published December 02, 2020 as 10.1165/rcmb.2020-0153OC
Copyright © 2020 by the American Thoracic Society

54. Albertine KH, Jones GP, Starcher BC, Bohnsack JF, Davis PL, Cho SC, et al. Chronic lung injury in preterm lambs. Disordered respiratory tract development. *Am J Respir Crit Care Med.* 1999;159(3):945-58.

55. Li J, Yu KH, Oehlert J, Jeliffe-Pawlowski LL, Gould JB, Stevenson DK, et al. Exome Sequencing of Neonatal Blood Spots and the Identification of Genes Implicated in Bronchopulmonary Dysplasia. *Am J Respir Crit Care Med.* 2015;192(5):589-96.

56. Hamvas A, Feng R, Bi Y, Wang F, Bhattacharya S, Mereness J, et al. Exome sequencing identifies gene variants and networks associated with extreme respiratory outcomes following preterm birth. *BMC Genet.* 2018;19(1):94.

AJRCMB Articles in Press. Published December 02, 2020 as 10.1165/rcmb.2020-0153OC
Copyright © 2020 by the American Thoracic Society

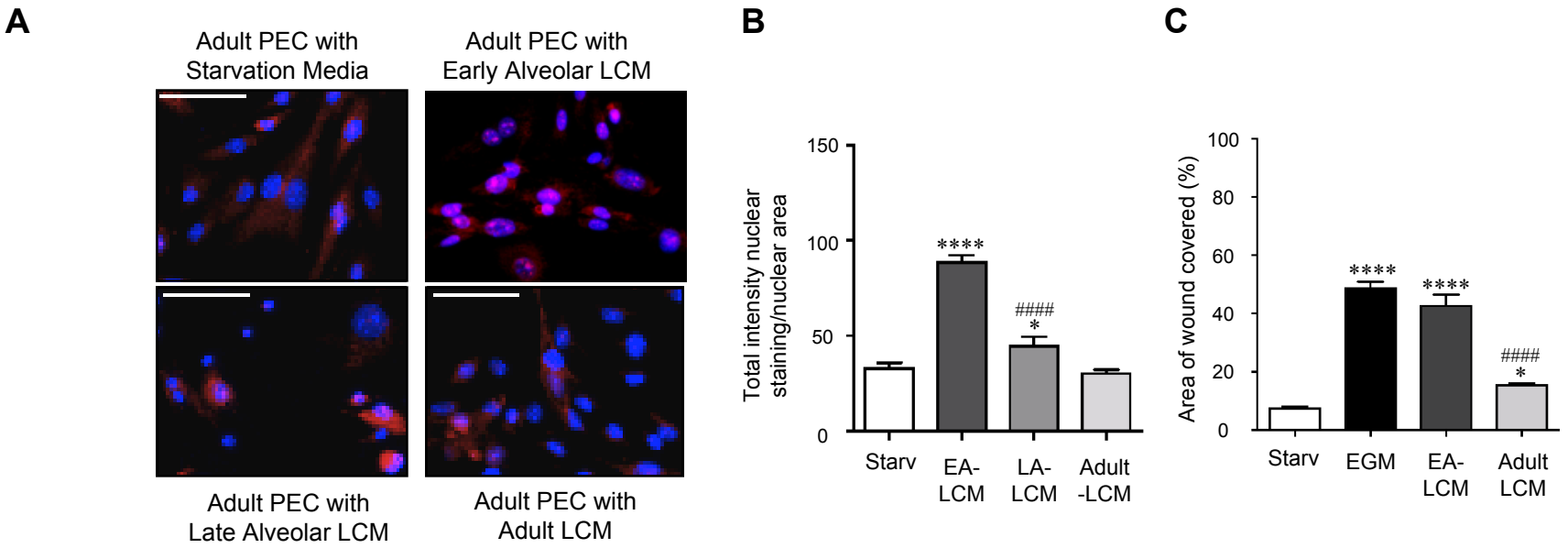

Figure 1

AJRCMB Articles in Press. Published December 02, 2020 as 10.1165/rcmb.2020-0153OC
Copyright © 2020 by the American Thoracic Society

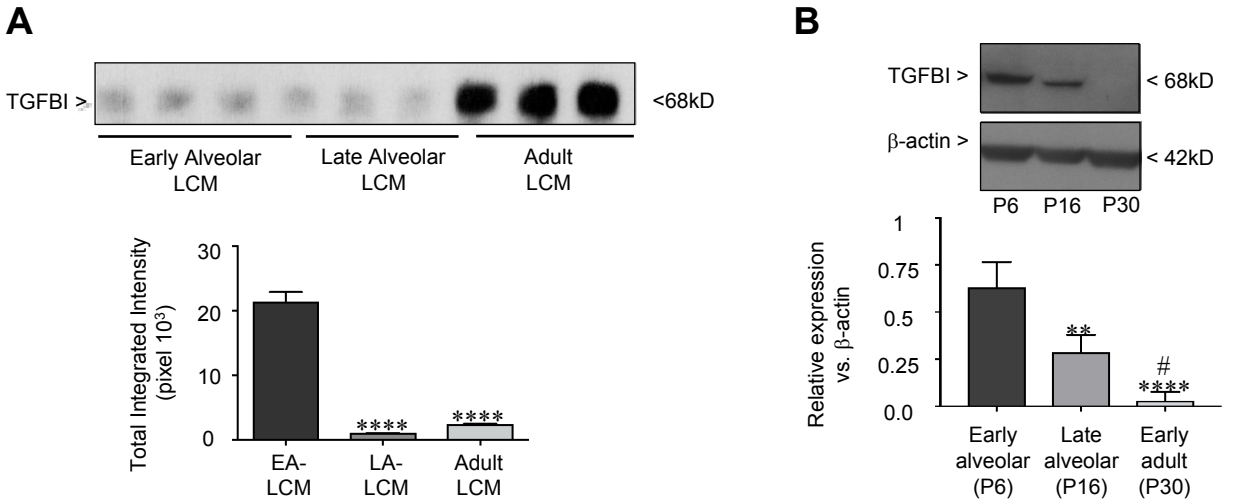

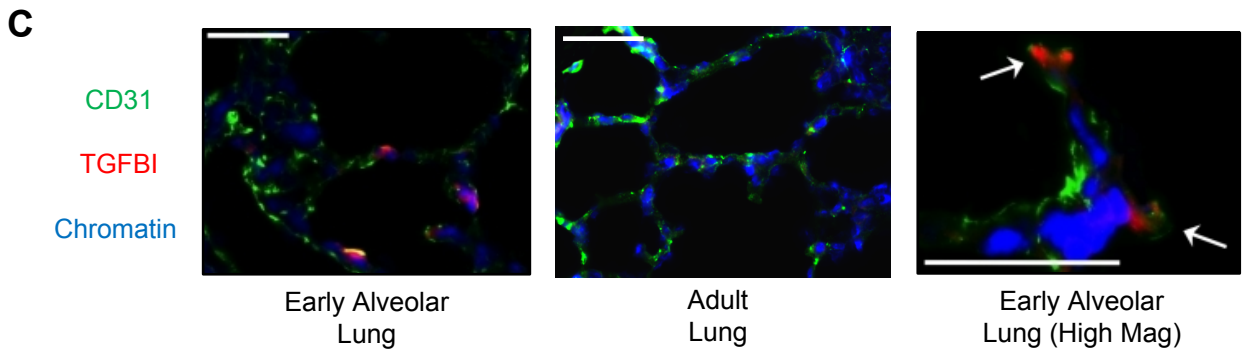

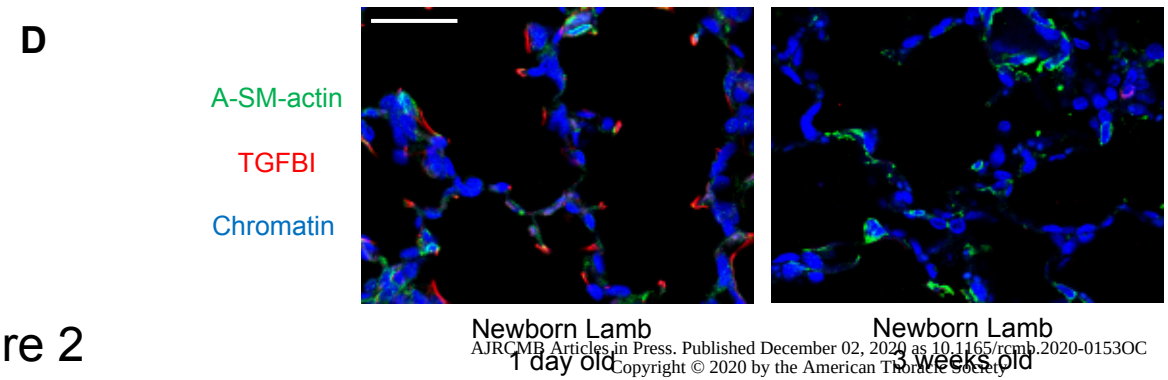

Figure 2

AJRCMB Articles in Press. Published December 02, 2020 as 10.1165/rcmb.2020-0153OC
Copyright © 2020 by the American Thoracic Society

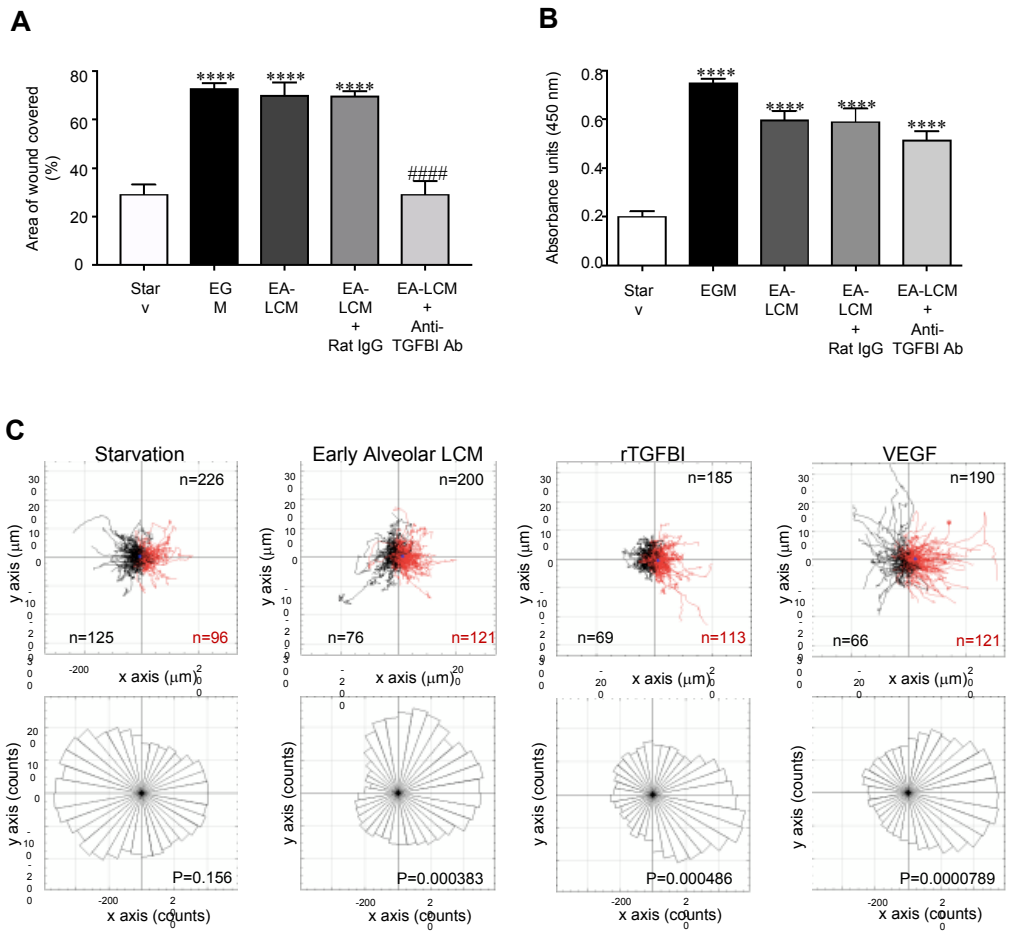

Figure 3

AJRCMB Articles in Press. Published December 02, 2020 as 10.1165/rcmb.2020-0153OC
Copyright © 2020 by the American Thoracic Society

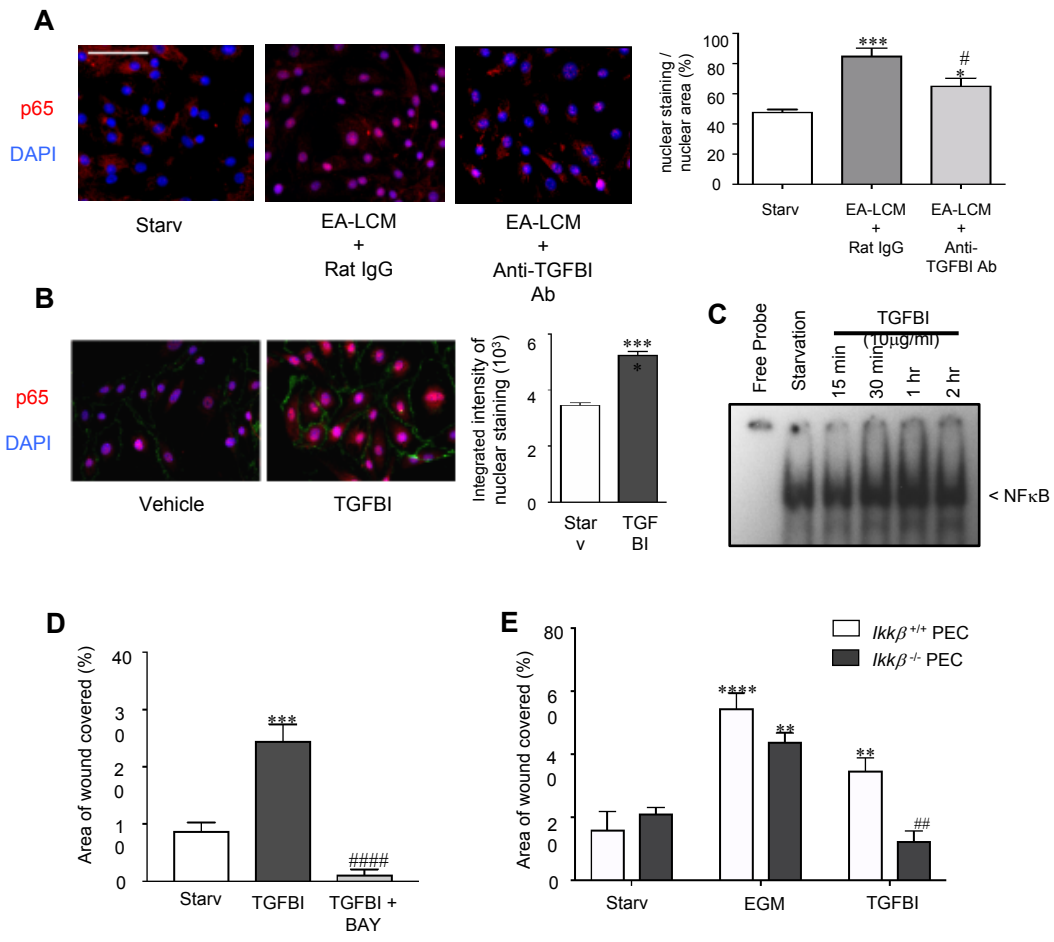

Figure 4

AJRCMB Articles in Press. Published December 02, 2020 as 10.1165/rcmb.2020-0153OC
Copyright © 2020 by the American Thoracic Society

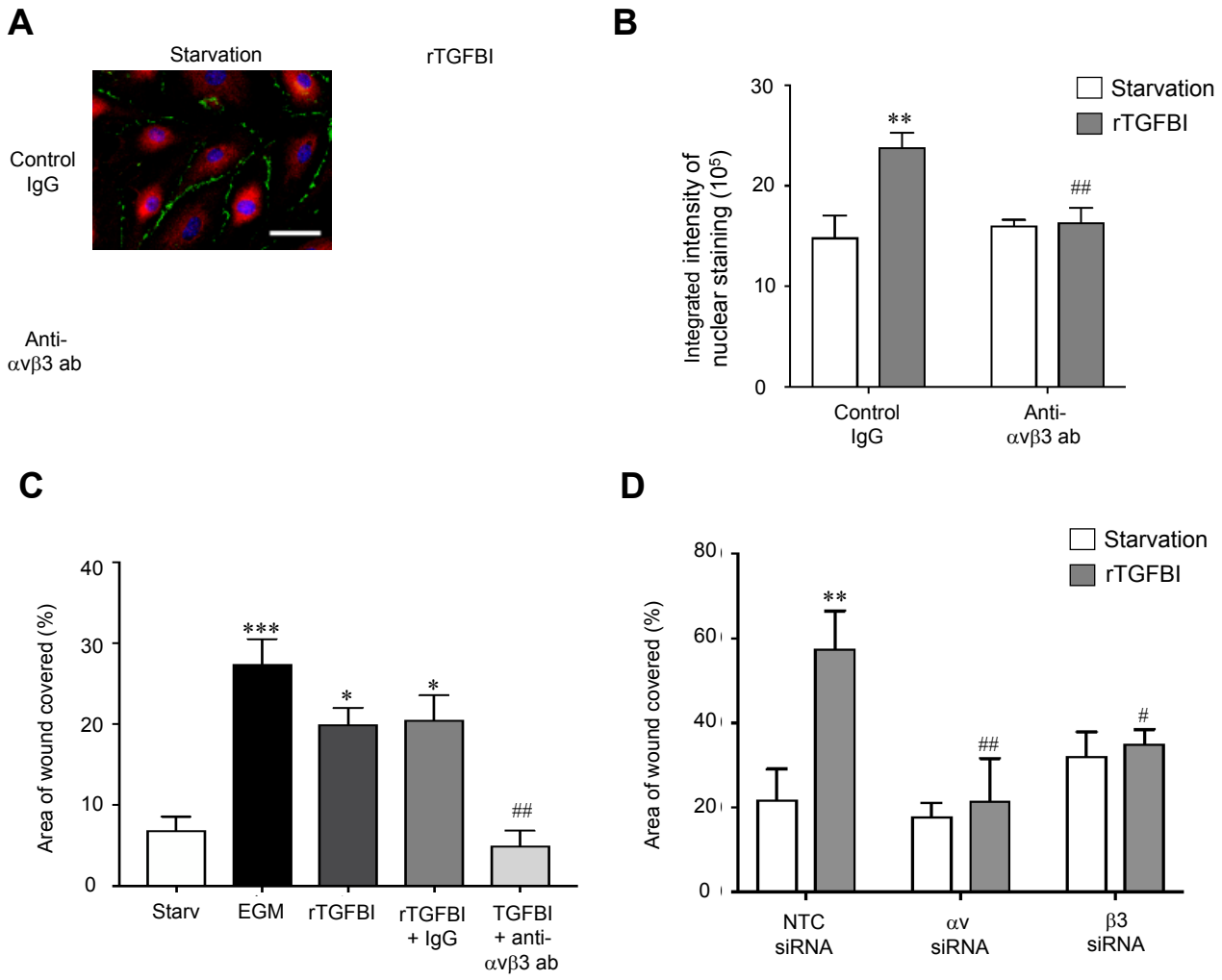

Figure 5

AJRCMB Articles in Press. Published December 02, 2020 as 10.1165/rcmb.2020-0153OC
Copyright © 2020 by the American Thoracic Society

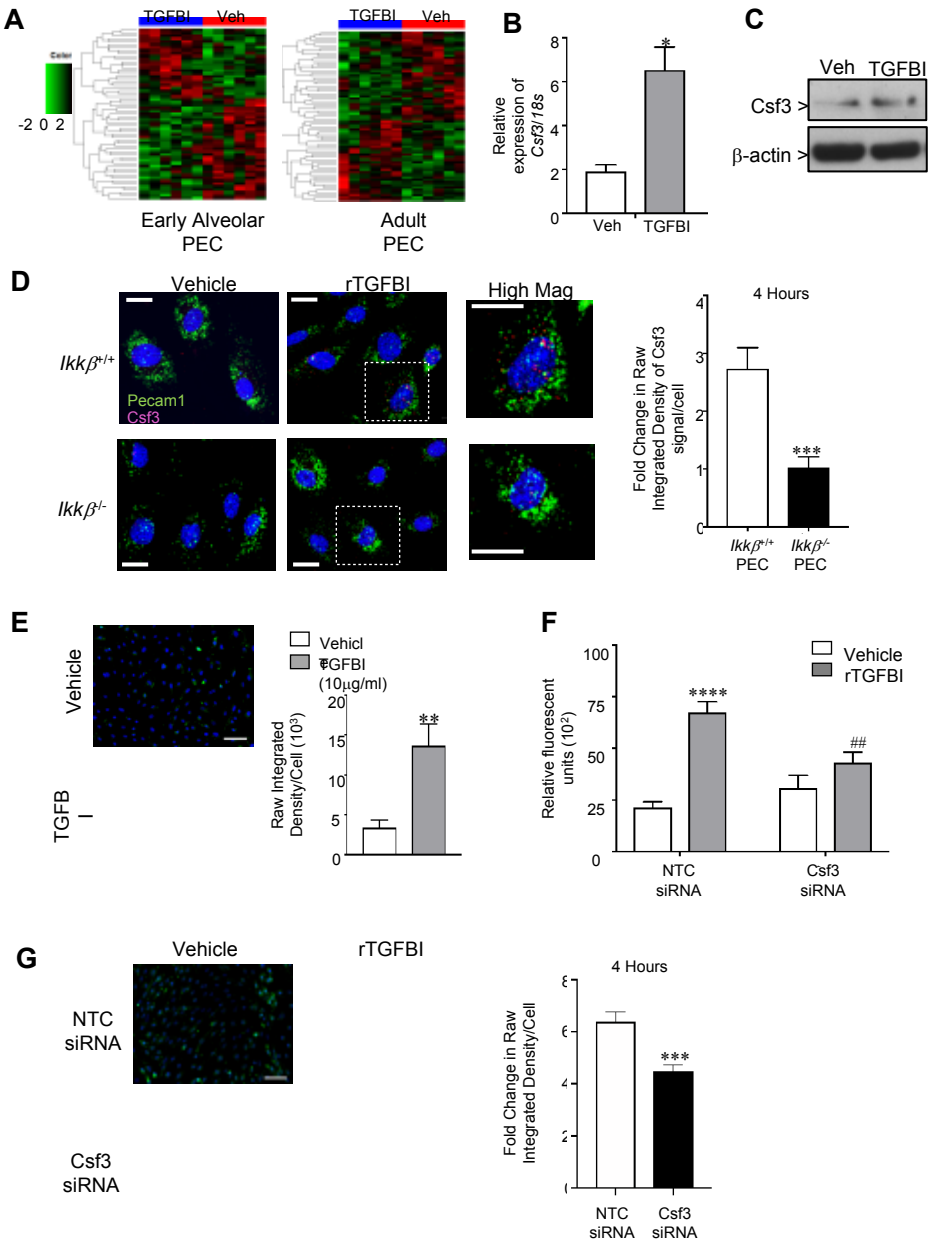

Figure 6

AJRCMB Articles in Press. Published December 02, 2020 as 10.1165/rcmb.2020-0153OC
Copyright © 2020 by the American Thoracic Society

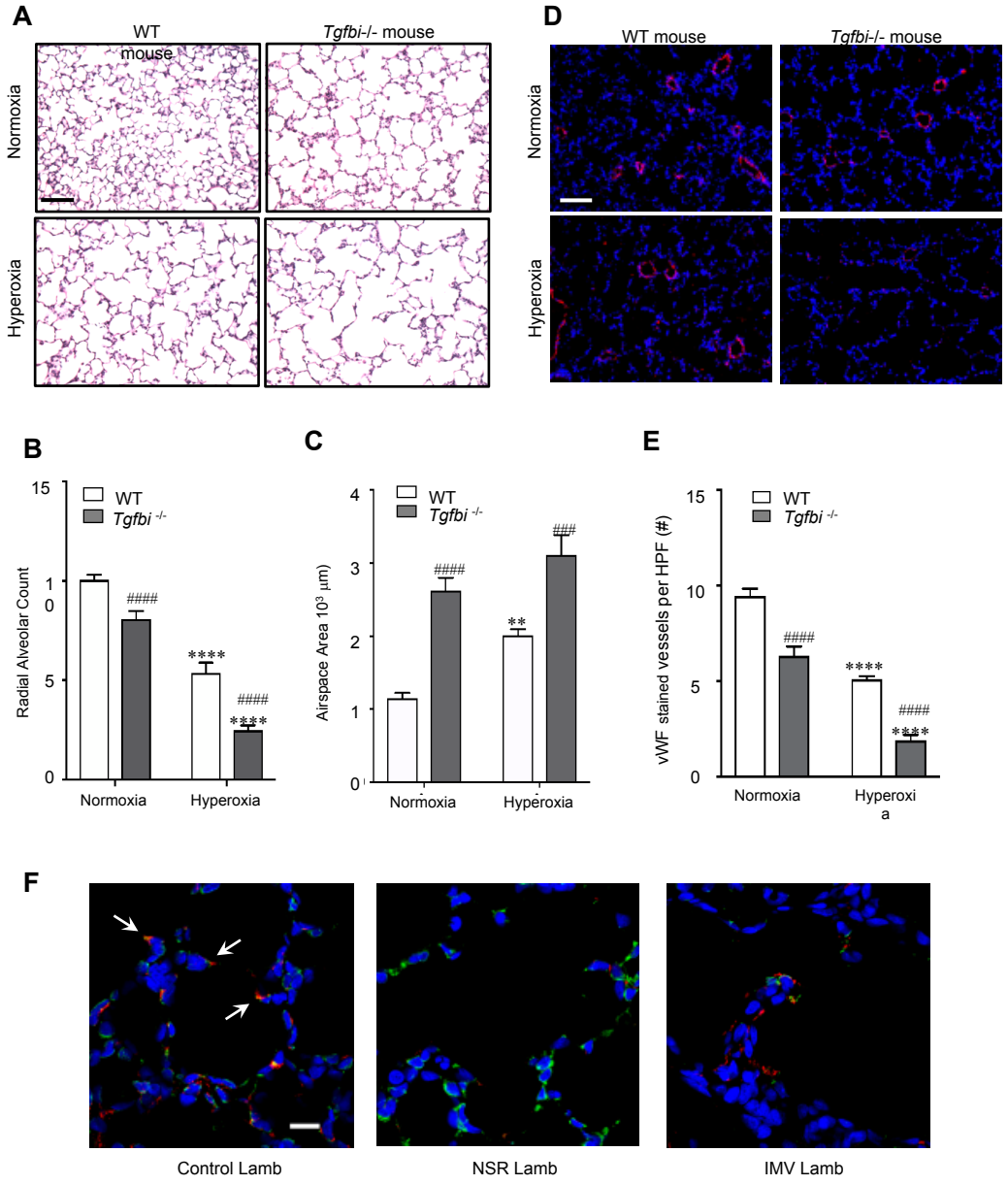

AJRCMB Articles in Press. Published December 02, 2020 as 10.1165/rcmb.2020-0153OC
Copyright © 2020 by the American Thoracic Society

Figure 7

Transforming Growth Factor Induced Protein Promotes NF-Kappa-B Mediated Angiogenesis During Postnatal Lung Development

Min Liu PhD, Cristiana Iosef PhD, Shailaja Rao PhD, Racquel Domingo-Gonzalez, Sha Fu MD, Paige Snider PhD, Simon J. Conway PhD, Gray S. Umbach MD, Sarah C. Heilshorn, Ruby E. Dewi, Mar J. Dahl, Donald M. Null MD, Kurt H. Albertine PhD, and Cristina M. Alvira MD.

ONLINE DATA SUPPLEMENT

AJRCMB Articles in Press. Published December 02, 2020 as 10.1165/rcmb.2020-0153OC
Copyright © 2020 by the American Thoracic Society

Methods:

Mice.

Neonatal mice at the early alveolar (postnatal day 6-P6) and adult male and female mice (10-12 weeks) C57BL/6 mice were purchased from Charles River Lab for the isolation of primary pulmonary endothelial cells. TGFBI null mice on a C57BL/6J background have been described previously (E1). Mice were interbred to generate TGFBI homozygotes and WT controls. Genotyping were done using primers 5'-TGTCCGTGCCTAAGTGTGAG-3' and 5'-CAGCAGCAGACCATTTTCAA-3' to detect null allele ~399bp; 5'-TCAACAGCCACAGTGAAAGG-3' and 5'-GCCTGTAACCATTTGCCACT-3' to detect wildtype allele ~520bp. Mice were maintained at 22±2°C and fed a standard diet of rodent chow and water ad libitum.

Preparation and Analysis of Lung Conditioned Media

The lung conditioned medium was prepared by incubating lung tissue from C5BL/6 mice at the early alveolar (P6), late alveolar (P16) and adult (8-10 weeks) stages of development in serum free EGM medium with antibiotics, at 37^0C in a 5% CO_2 incubator. Lung tissue was perfused with PBS and inflated with serum free media. The lung tissue was aseptically removed, minced, and weigh normalized by resuspension at a 4:1 media to tissue (vol/wt) ratio in serum free ECM medium with antibiotics. After 24h, the lung conditioned media (LCM) was collected, cleared by centrifugation, aliquoted and frozen at -80^o C until use. To account for mouse-to-mouse variability, LCM from multiple mice were pooled before use in the following experiment.

Protein extracts from all three LCM (P7, P10, Adult) were labeled with separate fluorescent proteins and co-separated on a single gel via IEM 2D-PAGE (Applied Biomics, Hayward, CA).

AJRCMB Articles in Press. Published December 02, 2020 as 10.1165/rcmb.2020-0153OC
Copyright © 2020 by the American Thoracic Society

Fluorescent signals from each pair of two samples were then visualized for a total of three comparisons. The gel images were processed using DeCyder establish the ratios of relative expression between each comparison of samples. Selected spots were subjected to in-gel digestion, and identification via mass spectroscopy. Data were processed using Mascot 2.1 (*http://mascot.bio.nrc.ca/*) or Micromass ProteinLynx Global Server 2.0. Peptide data were searched against the latest SwissProt database for protein identification.

Isolation of Primary Pulmonary Endothelial Cells (PEC)

PEC were isolated from P6 or adult C57BL/6 mice, from P6 TGFBI KO or WT mice, as described previously in our lab (E2, E3). Briefly, PECs were obtained from 10-12 mouse lungs by digestion of whole lung tissue with collagenase IA (0.5 mg/ml, Sigma, St. Louis, MO) for 30 min at 37°C, followed by incubating cell lysate for 15 min at RT with anti-CD31-coated magnetic beads (Dynabeads, Invitrogen, Carlsbad, CA), resulting in between 2-3 million PEC after bead selection. PEC isolated by this method were previously characterized by flow cytometry and found to be exclusively CD45- , greater than 95% positive for the endothelial specific marker, CD102 (E2), and greater than 80% demonstrating binding to Griffonia simplicifolia, indicating primarily microvascular EC. PEC were also isolated from mice containing an endothelial cell specific deletion of the NFκB activator *Ikkβ* by crossing $Ikk\beta^{fl/fl}$ mice (E4) with *Pdgfb*-iCre mice (E5). PEC were then cultured in endothelial growth media (EGM) containing 5% FBS with growth factors (EBM-2; Lonza, Basel, Switzerland) at 37°C in 5% CO_2. PEC from passage 0-2 were used for all experiments. In some studies, PEC were treated for 4h with either vehicle (DMSO) or the pharmacologic NFκB inhibitor, BAY11-0782 (2.5 μM), followed by TGFBI (10 μg/ml) treatment for 24h for wound healing assay.

AJRCMB Articles in Press. Published December 02, 2020 as 10.1165/rcmb.2020-0153OC
Copyright © 2020 by the American Thoracic Society

TGFBI Neutralization and Stimulation

Neutralization of TGFBI was performed by adding either isotype control antibodies (rat IgG, Cell Signaling Danvers, MA) or anti-TGFBI antibodies (LifeSpan BioScience, Seattle, WA) at a concentration of 4μg/ml prior to diluting the LMC 1:1 in starvation media (EGM + 0.2% FBS). For TGFBI stimulation experiments, cells were stimulated with vehicle (PBS) or recombinant TGFBI (R&D Systems, Minneapolis, MN) at a concentration of 10 μg/ml for all studies.

Inhibition of Integrin αvβ3 Signaling

Neonatal or adult PEC (6.5-7 x10^4 cells /well) from passage P1 were starved for 2 h, then anti-αvβ3 integrin antibody (4 μg/ml; Abbiotec, Escondido, CA) or isotype control (Cell Signaling, Danvers, MA) were added to each plate for 2h, followed by stimulation with TGFBI (10 μg/ml) for 24h for wound healing assays. For immunostaining of NFκB/p65, cells were plated and attached on the 22mm^2 coverslips placed in the 6-well plate overnight, and then stimulated with TGFBI (10 μg/ml) for 30 min before images were taken.

Immunocytochemistry to Assess NFκB Activity

PEC were grown on 22mm^2 coverslips placed in a 6-well cell culture plate until form a thin monolayer. Cells were fixed with 100% ethanol and air-dried. Cells were rehydrated and immunocytochemistry performed as previously described using primary antibodies against p65 (1:200; Santa Cruz Biotechnology, Santa Cruz, CA) overnight at 4° (E2). Fluorescent images were captured and quantified using either a Leica DM5500B Upright or Keyence BZ-X700/BZ-X710 Microscope, and Metamorph Image analysis software (Molecular Devices, Sunnyvale, CA).

AJRCMB Articles in Press. Published December 02, 2020 as 10.1165/rcmb.2020-0153OC
Copyright © 2020 by the American Thoracic Society

Chemotactic Migration Assays

Boyden chamber assays were done according to a standard protocol (E6). Starvation media +/- TGFBI were added into the lower chamber, and $1x10^5$ PEC were added to the insert in the upper chamber. Cells were incubated with TGFBI for 8h, at the experimental endpoints cells remaining in the inner side of the insert were removed and the insert was placed in medium containing 8μM Calcein AM for 45 min, trypsinized, and the fluorescence measured at excitation wavelengths of 485nm and 520 nm.

Endothelial Wound Healing Assays

PEC (6-7 $x10^4$) were incubated in EGM on 48-well plates for 48h. A linear wound was created using a sterile pipet tip, and the EGM media was then replaced with experimental media detailed in the figure legends. Phase contrast images were captured at time 0 and 24h post-treatment and the percentage of the wound area covered at 24h calculated for each experimental group. Images were taken from at least four wells of each experimental group and data were analyzed using Image J software (NIH).

Microfluidic Chemotaxis Assays

PEC migration was also assessed using microfluidic chemotaxis assays as previously described (E7). Microfluidic devices were fabricated using standard soft lithography and micromolding techniques at the Stanford Microfluidics Foundry clean room. The cell culture chamber was adsorbed with fibronectin overnight (10 μg/ml) and rinsed three times with buffer.

AJRCMB Articles in Press. Published December 02, 2020 as 10.1165/rcmb.2020-0153OC
Copyright © 2020 by the American Thoracic Society

PEC (1×10^6 cells/mL) suspended in starvation medium were injected into the cell culture chamber and allowed to adhere for ~3h. The inlet and outlet of the cell culture chamber were plugged, and tubing inserted into the inlets of the reagent channels and connected to syringes on a syringe pump (World Precision Instruments, Sarasota, FL). By supplying early alveolar conditioned medium, starvation media + rTGFBI (10μg/ml) or starvation media + VEGF (100 ng/ml) to the source reagent channel and starvation medium to the sink reagent channel (flow rate = 10 nl/min), a stable linear gradient of conditioning molecules is formed across the cell culture chamber. Migrating cells were tracked using time-lapse video microscopy (Zeiss Axiovert 200 microscope, Carl Zeiss AB, Stockholm, Sweden). Cells were imaged every 30 min for 750 min using a phase contrast 10X objective and AxioVision time-lapse software (Zeiss). For each condition, three independent trials were performed with ~60 migratory cell tracks recorded per trial. Cell-tracking analysis was performed using ImageJ software with MtrackJ plug-in. Directional histograms of migrating cells were generated using Chemotaxis and Migration Tool freeware (Ibidi, Munich, Germany), which generates a smoothed histogram for the number of cells migrating within a specific angular trajectory (angular bins of 10 degrees).

PEC Proliferation Assays

PEC proliferation was determined by BrdU incorporation assays. Neonatal and adult PEC (6×10^3) were plated into each well of a 96-well plate and synchronized with starvation media (0.2% FBS) for 16h, prior to stimulation with experimental media. The incorporation of BrdU was then measured by ELISA at 24h per the manufacturer's protocol (Roche Diagnostics, Mannheim, Germany).

AJRCMB Articles in Press. Published December 02, 2020 as 10.1165/rcmb.2020-0153OC
Copyright © 2020 by the American Thoracic Society

Western Immunoblot

Whole cell protein lysates were extracted from lung tissue or PEC using RIPA buffer. Proteins were then subjected to SDS-PAGE, transferred to PVDF membranes, and immunoblotting with primary antibodies performed as previously described (E3). The appropriate horseradish peroxidase-conjugated secondary antibody was used to detect the immune-complexes as enhanced chemiluminescence signals on Kodak X-ray films (GE Life Sciences, Piscataway, NJ). Western blots were processed and analyzed by Image J software (NIH).

Immunofluorescent Staining of Lung Tissue

Immunostaining was performed on formalin-fixed or frozen murine lung sections using techniques previously described (E2), probed with primary antibodies against CD31 (1:50 for frozen tissue; Abcam, Cambridge, MA; or 1:200 for fixed tissue; Dianova, Germany). TGFBI (sodium azide -free ,1:200; R&D system, Minneapolis, MN), NFκB p65 (1:100 Millipore, Billerica, MA) or von Willebrand factor (1:100; Millipore, Billerica, MA). In similar studies, premature lamb lung tissue was probed with a primary antibody against TGFBI (1µg/µl, Abcam, Cambridge, MA) and anti-alpha-smooth muscle actin (1:200, Sigma, St. Louis, MO). After staining, mouse slides were examined using a Leica DM5500 upright and a Micropublisher 5MPixel, color digital camera, using HC Plan Apo 25-mm objectives at 10X and 20X magnification (Leica Microsystems, Buffalo Grove, IL). The number of vWF positive vessels (diameter <100 µm) per high-powered field (HPF) was manually counted on 20X images in a blinded fashion. At least 10 non-overlapping fields per mouse were counted, and the number of vWF positive vessels per HPF averaged to give a single value per mouse. Lamb slides were examined using an inverted Zeiss LSM 780 multiphoton laser scanning confocal microscope (Carl

AJRCMB Articles in Press. Published December 02, 2020 as 10.1165/rcmb.2020-0153OC
Copyright © 2020 by the American Thoracic Society

Zeiss, Germany) with a Zen Black software. Image sizes were set to 1024 × 1024 pixels, and images were taken under the 63X high numerical-aperture oil immersion objective lenses. The excitation wavelength was 488 nm for alpha-SMA, 561 for TGFBI and 405 nm for DAPI.

Electrophoretic Mobility Shift Assays (EMSA)

Nuclear proteins were extracted from vehicle and TGFBI-treated early alveolar PEC using the NE-PER kit (Pierce, Rockford, IL). A total of 5ug of protein was used for binding reactions with γ−32P-labeled oligonucleotides containing the κB consensus sequence (Promega, Madison, WI) in a binding buffer containing 500 ng of salmon sperm DNA, 0.01 U of poly(dI-dC), and 0.5 mM DTT as described previously (E2).

RNA interference:

Early alveolar PEC at P6 were transfected with 25 nM of NTC, integrin αV, integrin β3, or Csf3 On-Target Plus SMART pool siRNA (Dharmacon, Lafayette, CO; Thermo Fisher Scientific, Lafayette, CO) using Lipofectamine 2000 (Invitrogen) for 6h as previously described (E8). The groups of PEC were then recovered for 42h, prior to use for Western immunoblot. In separate studies, siRNA-transfected PEC were stimulated with vehicle or recombinant TGFBI (10 μg/ml, R&D system, Minneapolis, MN) for 24h then followed by endothelial wound healing assays to assess PEC migration as described above.

RNA-Seq Analysis

AJRCMB Articles in Press. Published December 02, 2020 as 10.1165/rcmb.2020-0153OC
Copyright © 2020 by the American Thoracic Society

Early alveolar and adult PEC were cultured in EGM medium until passage 2, then starved overnight, prior to vehicle (PBS) or rTGFBI stimulation for 4h. Total RNA from vehicle and rTGFBI-treated cells were extracted using RNeasy Mini kit (Qiagen, Germantown, MD), and RNA-sequencing performed by Quick Biology (Pasadena, CA). Briefly, RNA integrity was confirmed by Agilent Bioanalyzer 2100, and libraries were prepared according to KAPA Stranded mRNA-Seq poly(A) selected kit (KAPA Biosystems, Wilmington, MA). Final library quality and quantity was analyzed and 150 bp paired end reads sequenced on Illumina HighSeq 4000 (Illumina Inc., San Diego, CA). Reads were mapped to the latest UCSC transcript set using Bowtie2 version 2.1.0 (E9) and the gene expression was estimated using RSEM v1.2.15 (E10). TMM (trimmed mean of M-values) was used to normalize the gene expression. Differentially expressed genes were identified using edgeR (E11). Genes showing altered expression with $p< 0.05$ and more than 1.5-fold change were considered differentially expressed.

Quantitative real time PCR

Total RNA was isolated from PEC treated with vehicle or rTGFBI using the RNeasy Mini kit (Qiagen, Germantown, MD). RNA (2 μg) was reverse-transcribed using Superscript III (Invitrogen), and qPCR was performed using TaqMan primers (Applied Biosystems, Carlsbad, CA) as described previously (E12). Quantification of target gene expression was performed using the Delta–Delta CT method and normalized to the expression of 18s.

Measurement of Nitric Oxide (NO) Production in PEC.

PEC were grown to 80% confluence, starved for 2h, and then stimulated with vehicle or rTGFBI for 4 or 24h. NO production was determined by loading the cells with 4-amino-5-

AJRCMB Articles in Press. Published December 02, 2020 as 10.1165/rcmb.2020-0153OC
Copyright © 2020 by the American Thoracic Society

methylamino-2',7'-difluorofluorescein diacetate (DAF-FM) (10 μM) (Invitrogen Molecular Probes) (E13) for 40 min at 37 °C, prior to immunofluorescent imaging as previously described (E14). Images were captured using a Keyence BZ-X700/BZ-X710 Fluorescence microscope with a cooled CCD camera (Keyence Corporation of America, IL). Fluorescence intensity of the images was quantified using ImageJ software (NIH). The ratio of total DAF fluorescence in the image to the total nuclei was used to normalize the variation in cell numbers in a particular field. Each experiment was repeated at least 3 times with more than six images taken per group for quantification.

Detection of Csf3 in PEC using RNAscope In Situ Hybridization (ISH)

To detect the expression of *Csf3* in PEC, we performed RNAscope ISH on PEC obtained from *Pdgfb*^{WT}-*Ikkβ*$^{fl/fl}$ *and Pdgfb*^{Cre}-*Ikkβ*$^{fl/fl}$ mice (E4, E5). PEC (1x 10^5 cells) at passage 1 were plated on 22 mm^2 coverslips and stimulated with rTGFBI for 4h. Cells were fixed in 10% formalin for 30 min and hybridized with in situ hybridization RNA probes targeting *Csf3* (1:50, Advanced Cell Diagnostics) and *Pecam1* (1:50, Advanced Cell Diagnostics, Newark, CA). Opal dyes (Opal 488, Opal 570, 1:1500, Akoya Biosciences, Menlo Park, CA) were used for signal amplification as directed by the manufacturer. Images were captured with Zeiss LSM 780 confocal microscopes, using 405nm, 488nm, and 560nm excitation lasers. Z-stacked confocal images were collected and processed by maximum intensity projection. Image analysis was done using ImageJ by quantification of the integrated density of *Csf3* particles in each single cell. For all quantification analysis, a cell was deemed positive if it contained >1 puncta per cell for a specific gene. All experiments were repeated for 3 times, with a total of n=9 used for data analysis.

Murine Model of BPD Induced by Chronic Hyperoxia

AJRCMB Articles in Press. Published December 02, 2020 as 10.1165/rcmb.2020-0153OC
Copyright © 2020 by the American Thoracic Society

Litters of newborn *Tgfbi*$^{+/+}$ and *Tgfbi*$^{-/-}$ pups at P0 were split into two groups and maintained in either room air (normoxia) or 80% O_2 (hyperoxia) in a BioSpherix chamber (BioSpherix, Parish, NY) for 14 days, an established experimental model that recapitulates the impaired alveolarization observed in bronchopulmonary dysplasia (E15). Dams were rotated every 24h to prevent oxygen toxicity. Pups were euthanized at P14 and lungs fixed with 4% paraformaldehyde at 25 cm H_2O pressure for histology. Morphometric analysis (radial alveolar count and airspace area and size) was performed as previously described (E2, E3).

Preterm Lamb Model of Impaired Alveolarization

The methods for delivery and continuous management of chronically ventilating preterm lambs are reported (E16-E19). Briefly, time-pregnant ewes that carried one fetus or twin fetuses at 132 ± 2 d of gestation (term ~150 d gestation) were used. The pregnant ewes were given dexamethasone phosphate ~36 h before operative delivery. At delivery, all preterm fetal lambs were intubated, administered Survanta before operative delivery, resuscitated by invasive mechanical ventilation (IMV), and given daily with postnatal caffeine citrate to stimulate respiratory drive. At ~3 h of age, the preterm lambs were randomized to continue IMV or transitioned to noninvasive respiratory support (NRS), provided by high-frequency nasal ventilation as previously described (E18) for a total of 21d. Control lambs were born at term and lived in the laboratory at the University of Utah Health Sciences Center.

Control and preterm NRS lambs were intubated and reconnected to the ventilator to maintain lung inflation when the chest was opened to remove the lungs. The whole left lung was insufflated with 10% buffered neutral formalin (static pressure of 25 cmH_2O), and immunofluorescence of paraffin-embedded lung sections performed as described above.

AJRCMB Articles in Press. Published December 02, 2020 as 10.1165/rcmb.2020-0153OC
Copyright © 2020 by the American Thoracic Society

Statistics

All data are presented as mean ± SEM. Statistical differences between two groups were determined by Student's t-test. Comparison between more than two groups was analyzed by One-Way (for one independent variable) or Two-Way ANOVA (for two independent variables), followed by Bonferroni Multiple Comparison post-hoc analysis. A P value of ≤ 0.05 was considered statistically significant.

Study Approval

Protocols for the murine and lamb studies adhered to American Physiological Society/US National Institutes of Health guidelines for humane use of animals for research and were prospectively approved by the Institutional Animal Care and Use Committee at Stanford University and the University of Utah Health Sciences Center.

AJRCMB Articles in Press. Published December 02, 2020 as 10.1165/rcmb.2020-0153OC
Copyright © 2020 by the American Thoracic Society

References

E1. Ahlfeld SK, Wang J, Gao Y, Snider P, and Conway SJ. Initial Suppression of Transforming Growth Factor-beta Signaling and Loss of TGFBI Causes Early Alveolar Structural Defects Resulting in Bronchopulmonary Dysplasia. *Am J Pathol.* 2016;186(4):777-93.

E2. Iosef C, Alastalo TP, Hou Y, Chen C, Adams ES, Lyu SC, et al. Inhibiting NF-kappaB in the developing lung disrupts angiogenesis and alveolarization. *Am J Physiol Lung Cell Mol Physiol.* 2012;302(10):L1023-36.

E3. Hou Y, Liu M, Husted C, Chen C, Thiagarajan K, Johns JL, et al. Activation of the nuclear factor-kappaB pathway during postnatal lung inflammation preserves alveolarization by suppressing macrophage inflammatory protein-2. *Am J Physiol Lung Cell Mol Physiol.* 2015;309(6):L593-604.

E4. Li ZW, Omori SA, Labuda T, Karin M, and Rickert RC. IKK beta is required for peripheral B cell survival and proliferation. *J Immunol.* 2003;170(9):4630-7.

E5. Claxton S, Kostourou V, Jadeja S, Chambon P, Hodivala-Dilke K, and Fruttiger M. Efficient, inducible Cre-recombinase activation in vascular endothelium. *Genesis.* 2008;46(2):74-80.

E6. Mastyugin V, McWhinnie E, Labow M, and Buxton F. A quantitative high-throughput endothelial cell migration assay. *J Biomol Screen.* 2004;9(8):712-8.

E7. Kuhnert F, Mancuso MR, Shamloo A, Wang HT, Choksi V, Florek M, et al. Essential regulation of CNS angiogenesis by the orphan G protein-coupled receptor GPR124. *Science.* 2010;330(6006):985-9.

AJRCMB Articles in Press. Published December 02, 2020 as 10.1165/rcmb.2020-0153OC
Copyright © 2020 by the American Thoracic Society

E8. Iosef C, Liu M, Ying L, Rao SP, Concepcion KR, Chan WK, et al. Distinct roles for IkappaB kinases alpha and beta in regulating pulmonary endothelial angiogenic function during late lung development. *J Cell Mol Med.* 2018;22(9):4410-22.

E9. Langmead B, and Salzberg SL. Fast gapped-read alignment with Bowtie 2. *Nat Methods.* 2012;9(4):357-9.

E10. Li B, and Dewey CN. RSEM: accurate transcript quantification from RNA-Seq data with or without a reference genome. *BMC Bioinformatics.* 2011;12:323.

E11. Robinson MD, McCarthy DJ, and Smyth GK. edgeR: a Bioconductor package for differential expression analysis of digital gene expression data. *Bioinformatics.* 2010;26(1):139-40.

E12. Alvira CM, Abate A, Yang G, Dennery PA, and Rabinovitch M. Nuclear factor-kappaB activation in neonatal mouse lung protects against lipopolysaccharide-induced inflammation. *Am J Respir Crit Care Med.* 2007;175(8):805-15.

E13. Montagnani M, Chen H, Barr VA, and Quon MJ. Insulin-stimulated activation of eNOS is independent of Ca2+ but requires phosphorylation by Akt at Ser(1179). *J Biol Chem.* 2001;276(32):30392-8.

E14. Rathel TR, Leikert JJ, Vollmar AM, and Dirsch VM. Application of 4,5-diaminofluorescein to reliably measure nitric oxide released from endothelial cells in vitro. *Biol Proced Online.* 2003;5:136-42.

AJRCMB Articles in Press. Published December 02, 2020 as 10.1165/rcmb.2020-0153OC
Copyright © 2020 by the American Thoracic Society

E15. Hilgendorff A, Reiss I, Ehrhardt H, Eickelberg O, and Alvira CM. Chronic lung disease in the preterm infant. Lessons learned from animal models. *Am J Respir Cell Mol Biol.* 2014;50(2):233-45.

E16. Reyburn B, Li M, Metcalfe DB, Kroll NJ, Alvord J, Wint A, et al. Nasal ventilation alters mesenchymal cell turnover and improves alveolarization in preterm lambs. *Am J Respir Crit Care Med.* 2008;178(4):407-18.

E17. Albertine KH, Dahl MJ, Gonzales LW, Wang ZM, Metcalfe D, Hyde DM, et al. Chronic lung disease in preterm lambs: effect of daily vitamin A treatment on alveolarization. *Am J Physiol Lung Cell Mol Physiol.* 2010;299(1):L59-72.

E18. Null DM, Alvord J, Leavitt W, Wint A, Dahl MJ, Presson AP, et al. High-frequency nasal ventilation for 21 d maintains gas exchange with lower respiratory pressures and promotes alveolarization in preterm lambs. *Pediatr Res.* 2014;75(4):507-16.

E19. Joss-Moore LA, Hagen-Lillevik SJ, Yost C, Jewell J, Wilkinson RD, Bowen S, et al. Alveolar formation is dysregulated by restricted nutrition but not excess sedation in preterm lambs managed by noninvasive support. *Pediatr Res.* 2016;80(5):719-28.

AJRCMB Articles in Press. Published December 02, 2020 as 10.1165/rcmb.2020-0153OC
Copyright © 2020 by the American Thoracic Society

Identification of Proteins Identified by Mass Spec and Relative Fold Change in Expression					
Spot ID	**Mass Spec ID**	**P6/ P16**	**P6/ P30**	**P16/P30**	**Subcellular Location**
2	Alpha-fetoprotein	6.7	5.8	-1.2	Secreted
3	Alpha-fetoprotein	5	2.4	-2.2	Secreted
4	TGF-β Induced Protein	2.2	9.1	4	Secreted/ECM
6	Alpha-enolase	2.7	3.8	1.3	Cytoplasm/Cell membrane
7	Bleomycin Hydrolase	3	2.2	-1.4	Cytoplasm
12	Isocitrate dehydrogenase (NADP)	2.5	11.3	4.3	Cytoplasm
16	14-3-3z	2.9	31.2	10.2	Cytoplasm
20	Stefin-1	2.3	9.7	4.1	Cytoplasm
21	Translationally-controlled tumor protein	2.2	15.8	6.8	Cytoplasm
36	Vimentin-N'-fragment	2.5	7.7	2.9	Cytoskeleton
38	Vimentin-fragment	2.1	7.9	3.6	Cytoskeleton
55	Purine nucleosidase phosphorylase	2.3	1.8	-1.3	Cytoplasm
59	ER resident protein 29	2.2	2.1	-1.1	Endoplasmic reticulum
64	Phosphoglycerate mutase 1	2.5	5.8	2.2	Cytoplasm/Nucleus
65	Collagen alpha-1 (III) chain	2.5	3.2	1.2	ECM
69	Calreticulin	7.3	4.3	-1.8	Cytoplasm/ ER
71	Stathmin	2.7	15.6	5.5	Cytoskeleton
75	Protein SET	2.6	5	1.8	Cytoplasm/ ER/ Nucleus
84	Transthretin	2.5	-1	-2.6	Secreted
87	Peptidyl-prolyl cis-trans isomerase	3.9	4.7	1.2	Cytoplasm

Supplemental Table E1. Identification of Proteins in the Lung Conditioned Media Identified by Mass Spectroscopy. Twenty proteins were selected for in-gel digestion and identification via mass spectroscopy. The relative expression of each protein spot on the 2D gel was determined by DeCyder and expressed as a ratio between each two samples, with P6 representing early alveolarization, P16, late alveolarization and P30, adult.

AJRCMB Articles in Press. Published December 02, 2020 as 10.1165/rcmb.2020-0153OC
Copyright © 2020 by the American Thoracic Society

TGFBI Regulated Genes in Early Alveolar Pulmonary Endothelial Cells					
Gene Name	**Fold Change**	**P value**	**Gene Name**	**Fold Change**	**P value**
Rn45s	2.38	1.76E-05	Tmsb15b2	4.17	0.0263
Csf3	3.01	0.0025	Wnk2	-1.70	0.0268
Kcne4	5.30	0.0026	A930024E05Rik	-1.70	0.0275
Gm5069	2.44	0.0039	Gsta1	4.26	0.0286
B130024G19Rik	2.29	0.0045	Gm10785	-2.32	0.0294
Gpr68	-1.87	0.0048	Hgd	-1.86	0.0311
Tmem26	-1.57	0.0050	4930539E08Rik	-2.07	0.0314
1700088E04Rik	2.19	0.0061	0610040B10Rik	-2.69	0.0324
Irx1	2.94	0.0076	Gm14391	-1.60	0.0327
D10Bwg1379e	-2.13	0.0088	Galnt14	2.51	0.0330
Mmp13	-2.03	0.0088	Guca1a	1.99	0.0335
Lekr1	-1.80	0.0094	Klra18	-1.53	0.0335
Ivl	3.22	0.0111	Fam184a	-1.93	0.0344
Vmn1r65	-1.63	0.0121	Gm20324	2.04	0.0360
Irg1	1.79	0.0137	Bicd1	-1.59	0.0365
B4galnt2	-2.61	0.0138	BC052688	-1.96	0.0379
Gm14378	-2.16	0.0140	Zfp345	-2.48	0.0385
Cxcl17	-2.65	0.0159	Wnt2b	1.55	0.0385
3110001I22Rik	-1.61	0.0164	Nkx2-1	2.04	0.0386
Gls2	1.83	0.0168	AW011738	-1.52	0.0392
Foxn1	2.87	0.0176	A930006K02Rik	2.13	0.0413
Syngr3	-2.12	0.0183	Fam229b	-1.57	0.0419
6030443J06Rik	-1.69	0.0201	Fam217a	-1.58	0.0442
Galr2	1.99	0.0210	Prg4	1.98	0.0449
4930431F12Rik	-1.88	0.0215	Pclo	-2.01	0.0458
Amd1	-51.49	0.0223	Nrip2	-2.26	0.0466
Catip	2.71	0.0226	Serpinb9g	2.94	0.0469
Pbld1	-2.37	0.0227	Egr3	-1.73	0.0474
Sel1l3	-1.80	0.0228	Epb4.1l4b	1.56	0.0492
Hpgd	-1.67	0.0251			

Supplemental Table E2. TGFBI Regulated Genes in Early Alveolar Pulmonary Endothelial Cells. Early alveolar PEC at passage 2 were starved overnight, and then stimulated with either vehicle or TGFBI (10 μg/ml) for 4h prior to RNA extraction for RNA sequencing. Differentially expressed genes with a fold change >1.5 and P value <0.05 were identified between TGFBI stimulated PEC and vehicle stimulated PEC.

AJRCMB Articles in Press. Published December 02, 2020 as 10.1165/rcmb.2020-0153OC
Copyright © 2020 by the American Thoracic Society

TGFBI Regulated Genes in Adult Pulmonary Endothelial Cells					
Gene Name	**Fold Change**	**P value**	**Gene Name**	**Fold Change**	**P value**
Nfkbiz	1.62	7.12E-06	Padi2	-2.21	0.0257
Tmem254c	-19.05	0.0004	Adrb3	-1.58	0.0257
A730098P11Rik	3.44	0.0005	1700001C19Rik	-2.05	0.0271
Pemt	-1.86	0.0011	Nog	-1.50	0.0276
Nr4a3	2.35	0.0016	Lgi4	-2.18	0.0282
Cxcl1	1.73	0.0017	Adamts18	2.01	0.0295
3110062M04Rik	-1.59	0.0017	A930013F10Rik	1.61	0.0307
Amd1	-28.01	0.0018	2810001G20Rik	-1.64	0.0307
Gm5643	3.45	0.0034	Eif3j2	8.10	0.0314
Lmcd1	-1.50	0.0036	1190002F15Rik	-1.53	0.0315
Zfp418	1.73	0.0042	Cdk5r1	-1.65	0.0315
Map3k8	1.61	0.0051	Rapgefl1	1.57	0.0327
Csf3	2.77	0.0053	Gm16973	1.52	0.0332
Tox3	2.64	0.0089	Matn3	2.00	0.0335
Gm6251	1.69	0.0091	Car15	2.08	0.0352
Angel1	-1.51	0.0094	Zfp54	1.53	0.0358
Cacna2d4	-2.78	0.0095	Vdr	1.65	0.0361
Rex2	-5.07	0.0107	Twist2	1.69	0.0363
Il6	1.63	0.0116	Zfp791	1.61	0.0380
2310039L15Rik	-1.94	0.0117	Pnp2	2.50	0.0389
Cd37	-2.33	0.0118	Gm13889	-1.51	0.0406
Aldh1b1	-1.52	0.0118	Slc29a2	-1.62	0.0406
Stc1	2.14	0.0125	Gm13826	2.40	0.0425
Sfxn4	-1.77	0.0130	Tagap	-2.69	0.0426
Hlf	1.80	0.0147	Lrrc29	-1.78	0.0435
Rasl11b	-1.53	0.0155	Zfp184	1.62	0.0439
Ccdc138	1.84	0.0205	Cnr2	-1.65	0.0454
Gem	1.62	0.0220	A930006K02Rik	2.09	0.0455
Pex11a	-1.86	0.0226	BC030307	-1.54	0.0468
Clec11a	-2.29	0.0241	Hist1h2ao	-1.50	0.0482
1190007I07Rik	-1.64	0.0250	Capn6	-2.42	0.0488
1110006O24Rik	-1.82	0.0253	4930528A17Rik	-1.86	0.0493
Cspg5	2.54	0.0254	5930403L14Rik	-2.60	0.0500
Zdbf2	2.28	0.0256			

Supplemental Table E3. TGFBI Regulated Genes in Adult Pulmonary Endothelial Cells. Adult PEC at passage 2 were starved overnight, and then stimulated with either vehicle or TGFBI (10 μg/ml) for 4h prior to RNA extraction for RNA sequencing. Differentially expressed genes with a fold change >1.5 and P value <0.05 were identified between TGFBI stimulated PEC and vehicle stimulated PEC.

AJRCMB Articles in Press. Published December 02, 2020 as 10.1165/rcmb.2020-0153OC
Copyright © 2020 by the American Thoracic Society

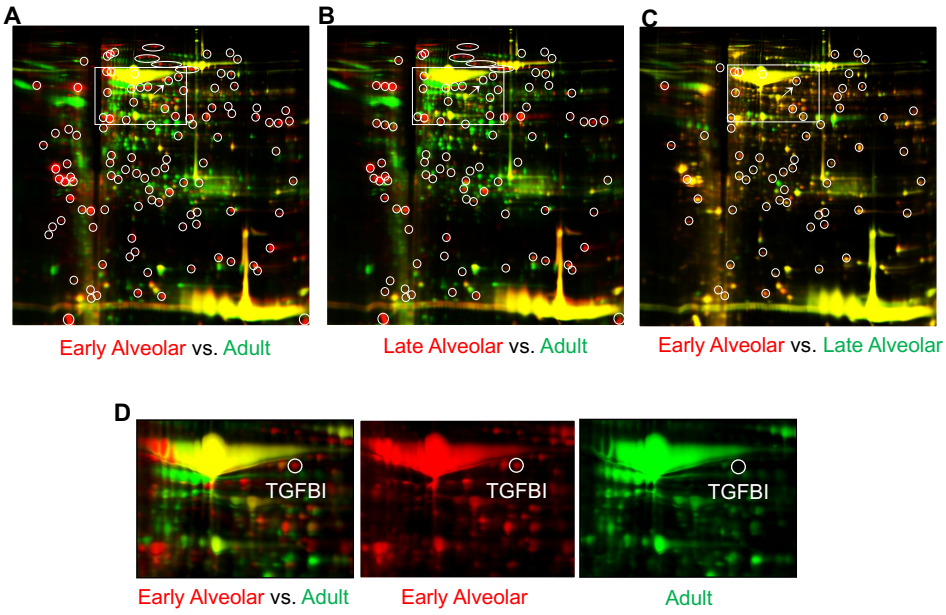

Figure E1. Proteomic analysis of lung conditioned media identifies TGFBI as a factor uniquely secreted by the early alveolar lung. Three separate fluorescent images of the same 2D gel after electrophoresis of proteins contained within the three LCM, imaged to compare the relative expression in each of the three comparison pairs: (A) early alveolar vs. adult; (B) late alveolar vs. adult; (C) early alveolar vs. late alveolar. In each comparison, proteins of one media are visualized in red and the protein of the other media visualized in green. Circled proteins were present in the early or late alveolar LCM but absent in the adult (A and B), and also increased in the early alveolar vs. the late alveolar LCM (C). Arrow points to the spot corresponding to TGFBI. (D) Enlarged image of the section of gel, containing the protein spot corresponding to TGFBI.

AJRCMB Articles in Press. Published December 02, 2020 as 10.1165/rcmb.2020-0153OC
Copyright © 2020 by the American Thoracic Society

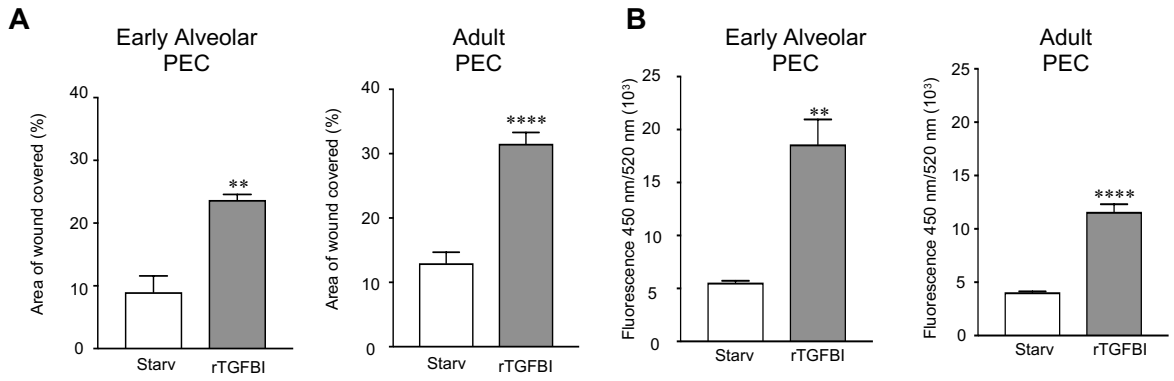

Figure E2. TGFBI is sufficient to promote early alveolar and adult PEC migration. (A) Endothelial scratch assays were performed using early alveolar and adult PEC incubated with starvation media or starvation media containing rTGFBI and the percent scratch area covered at 24h calculated. **P<0.01 and ****P<0.0001 vs. starvation with n=3 per group. (B) Boyden chamber assays in early alveolar and adult PEC incubated with starvation media or starvation media containing rTGFBI for 5h. **P<0.01 and ****P<0.0001 vs. starvation media with n=3 per group.

AJRCMB Articles in Press. Published December 02, 2020 as 10.1165/rcmb.2020-0153OC
Copyright © 2020 by the American Thoracic Society

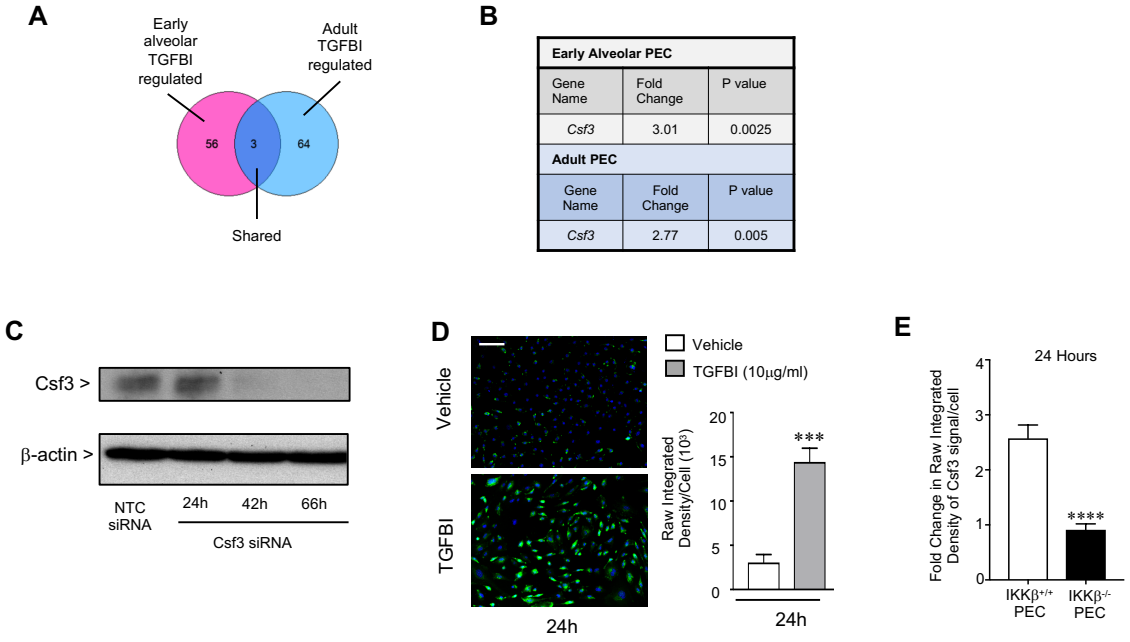

Fig. E3. TGFBI increases the expression of Csf3, a modulator of nitric oxide, in early alveolar PEC. (A) Venn diagram of unique and shared TGFBI-regulated genes in early alveolar and adult PEC. (B) *Csf3* is g up-regulated by rTGFBI in both early alveolar and adult PEC. (C) Representative western blot to detect CSF3 protein expression relative to β-actin in early alveolar PEC transfected with NTC and *Csf3* siRNA. (D) NO production assays in early alveolar PEC stimulated with starvation media containing vehicle or rTGFBI for 24h. Representative images taken to detect NO (green) and chromatin (blue). Calibration mark=100μm. Quantification of the raw integrated density of NO fluorescent signal per cell in early alveolar PEC stimulated with vehicle or rTGFBI for 24 hr. ***P=0.0002 vs. vehicle, with n=6-8 per group. Results are representative of 3 independent experiments. (E) Quantification of the fold change in raw integrated density of *Csf3* mRNA particles per cell compared to vehicle in $Ikk\beta^{+/+}$ and $Ikk\beta^{-/-}$ PEC treated with vehicle or rTGFBI for 24h. **** P<0.0001 vs. $Ikk\beta^{+/+}$ PEC with 10 replicates per group. Results are representative of 3 independent experiments.

AJRCMB Articles in Press. Published December 02, 2020 as 10.1165/rcmb.2020-0153OC
Copyright © 2020 by the American Thoracic Society